CHALMERS
UNIVERSITY OF TECHNOLOGY

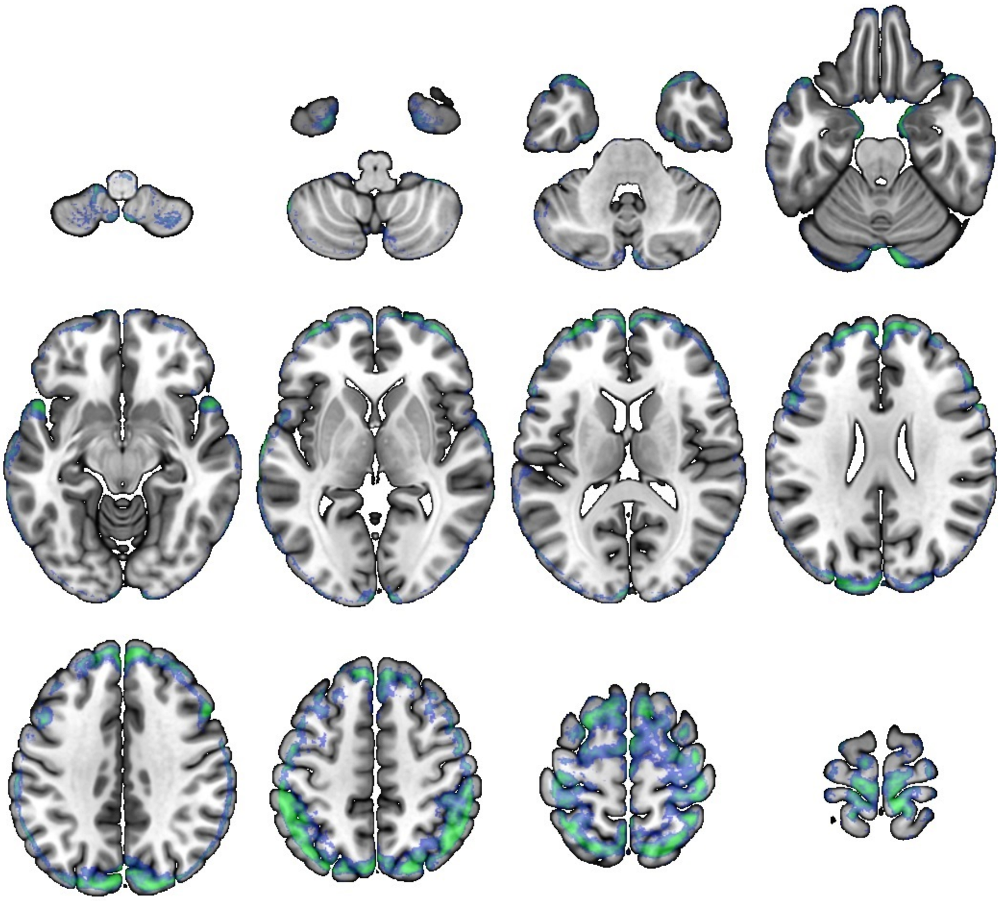

Developing and evaluating a novel tool for quantification and visualization of brain atrophy

Master's thesis in Biomedical Engineering

Emilia Gryska

Department of Signals and Systems

CHALMERS UNIVERSITY OF TECHNOLOGY
Gothenburg, Sweden 2017

Master's thesis EX082/2017

Developing and evaluating a novel tool for quantification and visualization of brain atrophy

EMILIA GRYSKA

CHALMERS
UNIVERSITY OF TECHNOLOGY

Department of Signals and Systems
Division of Signal processing and Biomedical engineering
Chalmers University of Technology
Gothenburg, Sweden 2017

Developing and evaluating a novel tool for quantification and visualization of brain atrophy

EMILIA GRYSKA

Supervisor: Rolf A. Heckemann, MD PhD, MedTech West at Sahlgrenska University Hospital University of Gothenburg
Examiner: Fredrik Kahl, Department of Signals and Systems at Chalmers University of technology

Master's Thesis EX082/2017
Department of Signals and Systems
Division of Signal processing and Biomedical engineering
Chalmers University of Technology
SE-412 96 Gothenburg
Telephone +46 31 772 1000

Cover: Visualization of cortical brain atrophy in Alzheimer's disease using MRIcroGL software (http://www.mccauslandcenter.sc.edu/mricrogl/).

Typeset in LaTeX
Gothenburg, Sweden 2017

Developing and evaluating a novel tool for quantification and visualization of brain atrophy
EMILIA GRYSKA
Department of Signals and Systems
Chalmers University of Technology

Abstract

Growing dementia incidence in aging societies brings about an increased need for biomarkers for differential diagnosis, monitoring, and assessing the effectiveness of candidate treatments. A promising path is to use imaging to search for characteristic patterns of regional brain atrophy in the various types of dementia and at various stages of disease progression. In this work, a novel approach is proposed that quantifies atrophy on magnetic resonance images of the brain by analyzing the discrepancy between the brain region and the cranial vault, the latter of which is assumed to represent the approximate premorbid brain volume. The atrophy on the regional level is estimated by segmenting the discrepancy region, labelling each voxel according to the nearest anatomical brain region. A complementary visualization of atrophy in the different types of dementia occurring in a clinical research database (the Gothenburg MCI Study) was produced. The results showed significant atrophy compared to controls in the following groups: Alzheimer's disease (AD), mixed-type dementia (Mix, featuring both vascular dementia and Alzheimer's disease), and a pooled group (MVD) containing both vascular and mixed-type dementia. Significantly atrophied regions were the superior temporal gyrus (middle part) and the inferior frontal gyrus in all three groups, the cuneus and the posterior orbital gyrus in AD and Mix, the angular gyrus and the third ventricle in AD and MVD, and the middle and inferior temporal gyrus and the lateral remainder of the occipital lobe in both Mix and MVD. The novel approach is not sensitive enough to distinguish between different dementia types, however its capability to indicate regions which are known for involvement in AD encourages further development of the method and more extensive validation.

Keywords: Alzheimer's disease, vascular dementia, biomarkers, MRI, brain atrophy

Acknowledgements

I would first like to thank my thesis supervisor, Prof. Rolf A. Heckemann for giving me the opportunity to work on this project and being my mentor. His great support, constant encouragement, and guidance have been a huge motivation to work hard and deepen my knowledge in the field of medical image processing and analysis. His enthusiasm, patience and readiness to help always inspired me to do my best and strive for a successful thesis project.
I would also like to thank Niklas Klasson for his advice and insightful comments about my project. His assistance helped me develop a deeper understanding of the subject and substantially contributed to the quality of my work.

Emilia Gryska, Gothenburg, September 2017

Contents

List of Figures

List of Tables

1
Introduction

Brain atrophy or shrinking can occur naturally due to aging, but it can also be a pathological process resulting from neurodegenerative diseases. Among these, the most prevalent are various types of dementia which lead to progressive deterioration in cognitive function. The brain regions affected by the disease vary depending on the dementia type [1–3]. Even though the causes of many diseases remain unknown, and the only available treatment alternatives mitigate the symptoms rather than curing the disease itself, an early and accurate diagnosis can have a huge impact on the life quality of patients and their carers.

Imaging biomarkers have emerged as a valuable tool in dementia research. Imaging is used for identification of the underlying pathologies, prediction and monitoring of the disease progression, and treatment response [11], [26]. Currently available imaging biomarkers focus on measuring relative change in patients' whole brain, and individual brain regions volume as a difference between consecutive measurements conducted between relevant time intervals. With the new approach explored in this thesis project, I aim to quantify the absolute change in brain volume as a difference between the cranial vault and brain volume. In this approach, an assumption is made that a healthy and fully developed brain occupies the whole volume outlined by the cranium. The purpose of the method is to assist and complement current diagnosis and progress tracking tools.

1.1 Motivation behind dementia research

The motivation for the research in the field lies in the scope of the dementia problem on a global scale. Increasing life expectancy in most of the developed countries results in aging population and an increased dementia incidence. Alzheimer's disease (AD) is the most common dementia cause responsible for 60-70% cases followed by vascular and Lewy body dementia (VaD, LBD) with 20-30 % of occurrence, and frontotemporal dementia (FTD) - 2% [4, 5]. According to the World Alzheimer Report from the year 2015 [6], 46.8 million people were estimated to be suffering from dementia and the count is expected to reach 74.7 million in 2030 and 131.5 million in 2050 worldwide. The percentage of individuals aged 60 and more who suffer from dementia was estimated to be 8.7 % in North Africa and Middle East, 7.6 % in North America and 4.7 % in Europe. The estimate for remaining regions falls in the range from 5.6 to 7.6 %. The collected data showed an exponential relation between dementia incidence and age, with the incidence doubling every 6.3 years. It is estimated that dementia incidence increases from 3.9 per 1000 people aged 60 to 64 to 104.8 per 1000 people aged 90 and more. Over the years it is expected that the dementia incidence will increase more in countries with low and middle income as compared to high income countries.

The likelihood of premature death is increased in neurodegenerative diseases, however, progressive deterioration in cognitive functions during the course of the disease creates distress for the patients and their caregivers during the years lived with dementia. Next to the huge impact dementia has on individuals, there is also a great societal and economical impact. In 2015, the global cost of dementia was estimated at US$ 818 billion, or 1.09 % of the global gross domestic product. By the year 2030, the global cost is estimated to more than double and amount to over US $ 2000 billion [6].

These projections suggest there is going to be an increased need for improved diagnostic tools. A breakthrough method would have a positive impact on many lives. Establishing a characteristic pattern of regional brain atrophy at various stages of disease progression is particularly important for discrimination between dementia types [26]. An accurate diagnosis allows patients and doctors to plan the medical care and explore the available treatment options. Pharmacological therapy often targets behavioural changes and aims to temporarily alleviate the psychological symptoms, which resemble those occurring in psychosis. Neuroleptic medications are often prescribed in AD or FTD [33, 34]. Those medications, however, were found to have adverse and potentially lethal effect in roughly 50 % of patients with LBD as well as increased disease advancement in some [5].

2

Theory

2.1 Imaging biomarkers in dementia

A biomarker is defined as a *"characteristic that can be objectively measured and evaluated as an indicator of normal biological or pathogenic process or pharmacological responses to a therapeutic intervention"* [9]. There are four main groups of biomarkers used in dementia diagnosis and research: neuropsychological, biochemical, genetic and neuroimaging [10]. Imaging biomarkers can be further divided into structural and functional, for which different modalities can be used. Most of the neuroimaging biomarkers successfully used in dementia research are based on volumetric analysis of the whole brain as well as its anatomical structures. Among various imaging modalities used in the field, MRI is advantageous in terms of safety, high spatial resolution, and strong contrast between cerebrospinal fluid, gray matter, and white matter [26].

No disease-modifying treatment is currently available, However, massive research efforts are underway, and candidate treatments are under pre-clinical investigation. To evaluate these treatments once they reach the stage of clinical trials, sensitive biomarkers will be needed to accurately assess their clinical value. These would ideally be applicable at the stage of subjective and mild cognitive impairment (SCI and MCI), because pathological changes during these early stages are more likely to be reversible. It is estimated that 50 to 70 % of elderly individuals suffering from MCI convert to AD within 5 to 7 years. Identifying patterns of atrophy that characterize the disease at this stage would lead to particularly valuable biomarkers [29].

2.1.1 Alzheimer's disease, mild and subjective cognitive impairment

Differential diagnosis is a challenge in case of dementia, since distinct types of neurodegenerative diseases result in similar signs and symptoms. While a number of studies have shown potentially indicative regional cortical atrophy associated with a particular type of dementia [5, 26–28, 30, 31], many parallels as well as inconsistencies have also been reported. In AD, the structures found to be affected include the medial temporal lobe region (hippocampus, entorhinal cortex), frontal gyrus and insula. Reduced hippocampus and medial temporal lobe (MTL) volumes measured with the help of MR imaging are considered fundamental AD biomarkers. The measure is characterized by high sensitivity; however, it is not discriminative without considering neuropsychological evaluation [40]. Atrophy of posterior brain regions, including precuneus and posterior cingulate gyrus, is observed early during AD. As the disease progresses, parietal and occipital lobes become affected. In comparison to other common dementia types, more rapid brain atrophy is expected in AD [26], [27], [31]. The results obtained by image segmentation correspond to those found in postmortem examinations of demented patients [1]. Hippocampal volume reduction has repeatedly been shown to predict conversion to AD in patients with MCI. Similarly, patients with subjective memory impairment who do not have signs of dementia are prone to developing AD, and the atrophy pattern resembles that of AD [44–47].

2.1.2 Lewy body dementia

A distinct atrophy pattern has not been established for LBD. Many studies have shown similarities to AD atrophy, including medial temporal lobe shrinkage, however, the changes are less extensive in LBD. The respective volumes of a whole brain, frontal and temporal lobes, hippocampus are amygdala are consistently smaller in AD than in LBD [5, 30, 31, 35]. Some authors report that only temporal lobe and hippocampus volumes in LBD patients differed significantly from controls [5, 30]; others found no significant difference between LBD and control subjects [36]. Other sources have shown that putamen, basal forebrain and substantia innominata shrink more in LBD than in AD [37–39], while caudate nucleus shrank at the same rate in both AD and LBD patients [24].

2.1.3 Vascular dementia

Vascular dementia is known to involve predominantly white matter (WM) changes [12, 59], however, cortical atrophy is also observed. Various studies show similarities between VaD and AD in terms of which regions are most affected. In particular, these are medial temporal lobe including hippocampus. These changes can occur on account of large-vessel ischemic strokes, which are among the most common cerebrovascular diseases. The atrophy is not as distinct as in AD, but considerably higher than in control subjects. Cerebral small vessel disease is another condition which can lead to VaD. The cerebellum and the brainstem are among the affected regions [25]. Also, the overall brain atrophy was reported greater in VaD as compared to controls [5, 43]. It is unclear, however, whether these changes are solely caused by processes occurring due to VaD, or by coexisting AD, or even by normal ageing. Mixed-type dementia is common especially in older patients [43].

2.1.4 Frontotemporal dementia

Finding a distinctive atrophy model in FTD is difficult because several variants of this type of dementia exist. The main subcategories are the behavioural (bvFTD) and language-affecting variants. The latter include primary progressive aphasia (PPA) and semantic dementia (SD), which is also sometimes classified as a subtype of PPA. The cortical atrophy rates and patterns in FTD vary with each variant [26,41]. While bvFTD affects mostly frontal regions of the brain, PPA/SD also involves the temporal cortex with higher atrophy rates than bvFTD in a visual assessment of patients' MR images [41]. Clinical findings attribute symmetrical changes in mesial frontal cortex, orbitofrontal cortex and anterior insula with progression to other frontal structures, striatum, hippocampus, posterior insula, and parietal lobe to the behavioural variant of FTD. In aphasia, a dominant, left-sided atrophy is observed in anterior temporal lobe (polar and perirhinal cortex, and anterior fusiform gyrus) [26]. A differential diagnosis between FTD and AD mostly concerns anterior cortex, since temporal lobe is notably affected in AD. Hippocampal atrophy, which is often proposed as an AD biomarker, is also found in FTD but the overall medial temporal lobe atrophy is not as pronounced as in AD [40].

A summary of regional atrophy occurring in different dementia diseases found by various studies is presented in Table 2.1

AD	**LBD**	**VaD**	**bvFTD**	**PPA/SD**
MTL	MTL	MTL	mesial front. cortex	ant. TL^L
hippocampus	hippocampus	hippocampus	hippocampus*	polar cortex^L
entorhinal cortex	TL	cerebellum	orbitofrontal cortex	perirhinal cortex^L
front. gyrus	putamen	brain stem	ant. insula	ant. fusiform gyrus^L
insula	basal forebrain		striatum*	
precuneus	substantia innominata		post. insula*	
caudate nucleus	caudate nucleus		PL*	
post. cingulate gyrus				
PL*				
OL*				

Table 2.1: Most atrophied regions found in various types of dementia; MTL – medial temporal lobe, post. – posterior, ant. – anterior, front. – frontal, * – regions found in progressed disease, ^{L} – left-sided atrophy, TL, PL, OL – temporal, parietal and occipital lobe respectively

2.2 Image segmentation

Volumetric analyses of the brain and its subregions require the application of segmentation procedures which delineate intracranial structures of interest. The proposed method uses existing tools: pincram [19] for brain and intracranial volume segmentation and MAPER [23] for segmentation of the brain into anatomical regions. These tools are applied to each of the subjects' MR images to obtain the intracranial volume (ICV) and brain binary masks (pincram), and anatomical brain segmentation (MAPER) consisting of 95 regions, which are used as input for the proposed method [23, 49–51].

2.2.1 pincram

The brain extraction tool – pincram – uses an iterative atlas-based segmentation to obtain an accurate label of the brain and intracranial volume. Atlas based segmentation employs a set of images with previously segmented masks (usually a verified automatic or expert manual segmentation) which are registered to a target image. An consensus mask is created according to a chosen voting rule for each voxel. Three levels of segmentation refinement were obtained at each of the three consecutive image registration types (rigid, affine, and non-rigid) to create the final brain label. The image registration procedure maximized normalized mutual information (NMI, Appendix A) between a target and a reference (atlas) image. The first registration level consists of rigid translation and rotation (6 degrees of freedom - DoF, Appendix A). The second level additionally allows shearing and scaling (12 DoF, Appendix A). The last level, a nonrigid registration uses deformation grid of points with a 6 mm spacing and B-splines as basis functions (10^6 DoF, the registration algoithms explained in [20, 22, 53]).

At each of the three registration levels, $l = 0$, 1 and 2, the following procedures are applied:

(1) registering n_l available atlases to the target image,

(2) summation of n_l available atlases to create a fuzzy mask F_l,

(3) thresholding F_l at t_l to create a boundary M_l for optimal registration parameters search at $l + 1$ level,

(4) thresholding F_l by setting voxels with intensity between 15 and 99 % to 1 and remaining to 0 to obtain a brain label C_l at the level l,

(5) choosing atlases to be used in the subsequent level that are most similar to the target; they are contained in the M_l mask extended by 4 voxels. To ensure an optimal selection of atlases as well as to provide at least 7 atlases for each stage, n_{l+1} is calculated as $max\{n_l \sqrt[3]{8/n_0}, 7\}$.

In the first level, all available atlases n_0 are used. The thresholds for the third step of each level were set as follows: $t_0 = 56\%$, $t_1 = 60\%$ and $T_2 = 60\%$ [19]. Sample results of brain and ICV masks obtained by pincram are shown in Figures 2.1 and 2.2 respectively.

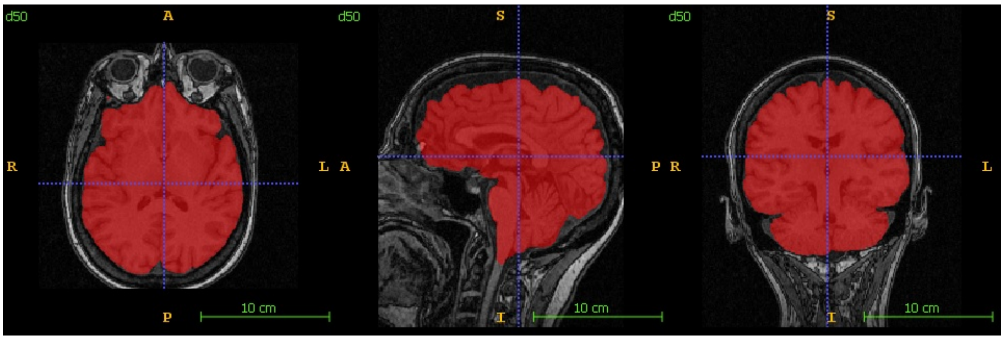

Figure 2.1: A sample brain mask obtained by pincram from an MRI scan; axial, sagittal and coronal view.

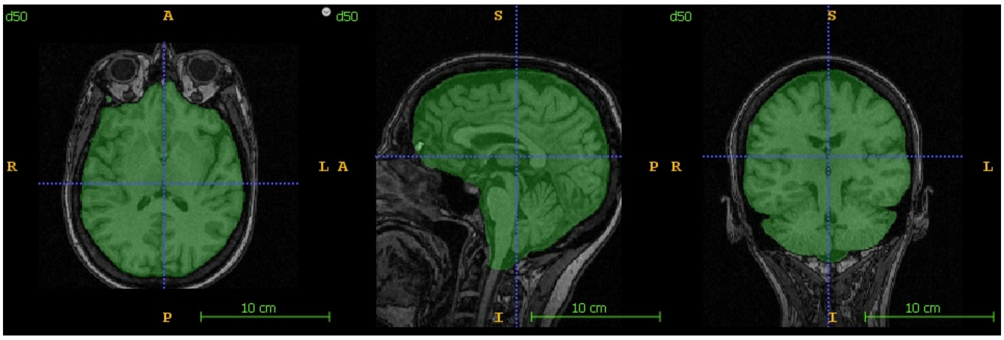

Figure 2.2: A sample ICV mask obtained by pincram from an MRI scan; axial, sagittal and coronal view.

2.2.2 MAPER

Anatomical brain segmentation of each subject's MRI scan was achieved using multi-atlas propagation with enhanced registration (MAPER). The algorithm uses an atlas database of MR brain images that typically have been delineated manually. The atlases are aligned to the target image in a hierarchical image registration approach with 6 levels of refinement: rigid, affine and 4 resolutions of a free-form deformation based on cubic B-splines (20 mm, 10 mm 5 mm and 2.5 mm). Tissue probability maps (gray matter, white matter and cerebrospinal fluid) of the target and atlas images are used for the coarse registration steps up to 20 mm nonrigid registration (Figure 2.3).

In the remaining three nonrigid registration steps, NMI is applied between the skull-stripped MRI target image and the atlas images. For a given voxel in the target image, a consensus segmentation is obtained by taking a modal value of the corresponding voxels in the 30 registered atlases. The atlases were obtained from the publicly available Hammers_mith database that contains T1-weighted images of 30 young healthy adults that have been segmented into 95 anatomical regions by experts [23, 49–51]. An example of a MAPER brain segmentation result is shown in Figure 2.4.

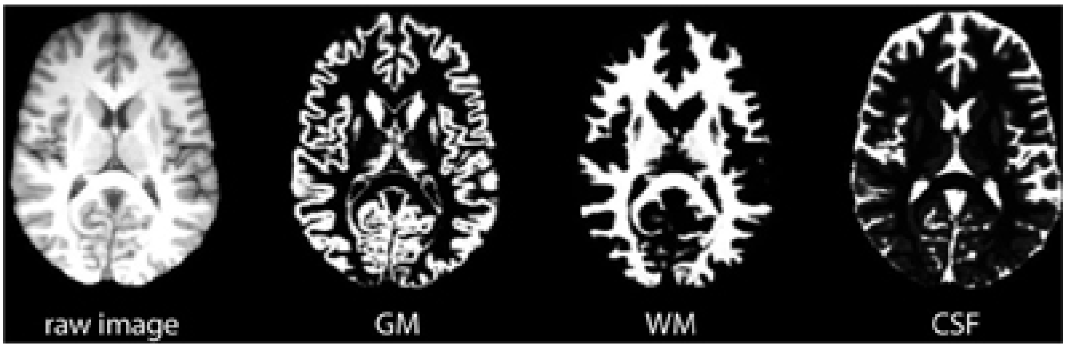

Figure 2.3: An example of a brain tissue probability map; GM - gray matter, WM - white matter, CSF - cerebrospinal fluid [52].

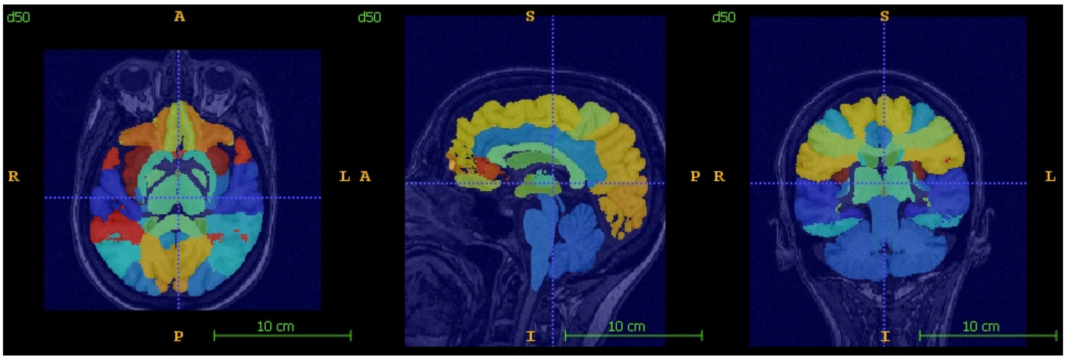

Figure 2.4: A sample anatomical region brain segmentation obtained by MAPER from an MRI scan; axial, sagittal and coronal view.

3

Materials and methods

3.1 Study cohort

The data used in the current project comes from the Gothenburg MCI Study [59], which comprises patients referred to a memory clinic as well as healthy controls. The cognitive functions of each patient were evaluated by four diagnostic procedures and categorized based on a four-stage global deterioration scale (GDS) [59, 60], (Stage 1 – healthy, Stage 2 – subjective cognitive impairment (SCI), Stage 3 – MCI, and Stage 4 - dementia). Stage 4 patients were further diagnosed as: Alzheimer's disease (AD), vascular dementia (VaD), AD+VaD (Mix [mixed-type dementia]), frontotemporal dementia (FTD), non-specified dementia (NUD), primary progressive aphasia (PPA), Lewy-body dementia (LBD), and FTD+VaD (Mix FTD/VaD). The Gothenburg MCI study examinations include longitudinal data of some individuals. In this project, however, only the baseline scans or the earliest available scans (if the baseline examination did not include an MR scan) were analyzed to avoid overestimation of the method's ability to distinguish between different dementia types. Some scans were also considered unsuitable for the processing tools used in this study. The resultant subset of images for this project consisted of 512 MR scans of individuals over 50 years of age, out of which 40 were healthy controls and the remaining patients were classified as follows: AD = 64, Mix = 32, VaD = 14, NUD = 38, FTD = 3, LBD = 1, Mix FTD/VaD = 1, PPA = 1, MCI = 165, SCI = 139 and not demented (ND) = 14. Each MR scan was a T-1 weighted MR image acquired on a 0.5-T Philips NT5 scanner (years 1999 - 2004) or a 1.5-T Siemens Symphony system (from year 2005). A focus of the Gothenburg MCI study is to identify characteristics which could contribute to discriminating between Alzheimer's disease and vascular dementia. The number of patients diagnosed with VaD is not sufficient to make a significant inference about the group. To improve statistical power I combined the VaD and Mix groups, despite the presence of AD pathology in the mixed type of dementia. The diagnosis protocol for AD, Mix and VaD classifies them based on white matter changes – mild, moderate or severe – and presence or absence of signs and symptoms associated with degeneration of particular brain lobes. AD classification allows no or mild WM changes with dominant parietotemporal clinical presentation. Vascular dementia involves dominant frontal lobe signs and symptoms and all stages of WM changes. Mixed-type dementia is diagnosed when aside from parietotemporal lobe symptoms (which are included in the clinical criteria for AD), moderate or severe white matter changes are present without distinct frontal lobe symptoms, or when mild white matter changes co-occur with frontal lobe symptoms [59].

The detailed demographic information of the subset included in this project is presented in Table 3.1.

Group	**n**	**Mean age (years) ± SD**	**F/M**
control	40	61.8 ± 6.3	23/17
AD	64	67.6 ± 6.8	37/27
Mix	32	71.3 ± 6.2	23/9
VaD	14	69.2 ± 6.9	3/11
NUD	38	67.5 ± 6.4	12/26
FTD	3	55.3 ± 4.04	2/1
LBD	1	74 ± 0	1/0
Mix FTD/VaD	1	70 ± 0	1/0
PPA	1	65 ± 0	1/0
MCI	165	66.6 ± 7.7	92/73
SCI	139	63.5 ± 7.7	88/51
ND	14	59.1 ± 10.9	9/5
VaD + Mix	46	70.7 ± 6.5	26/20

Table 3.1: Detailed information about the study participants; n - number of subjects, SD - standard deviation, * - years, F/M - females/males

3.2 Method design

The starting point for the approach was the assumption that a healthy and fully developed brain occupies approximately the whole intracranial volume (ICV). A visual examination of MR scans of both demented as well as healthy elderly individuals reveals a discrepancy between the ICV and the brain volume at the time of examination. Neurodegenerative diseases as well as processes observed in normal aging account for most of the disparity between those two volumes. The discrepancy region (DR, Figure 3.1) is acquired by subtracting the brain mask from the ICV mask (Section 2.2.1). A consecutive segmentation of the DR by labelling its voxels by the proximity to the anatomical brain regions (MAPER, section 2.2.2) produces an estimate of a premorbid brain structure. Volumetric analysis of the segmentation allows the quantification of the extent of cortical atrophy and evaluation of involvement of individual brain regions adjacent to the DR.

The key issues addressed in this project consisted of (1) developing an algorithm for an accurate and time-efficient DR segmentation, (2) implementing suitable statistical methods to analyse volumetric data acquired in the segmentation process, (3) creating a cumulative atrophy distribution visualization for each dementia group in the form of a heat map (atrophy heat map – AHM), and finally (4) verifying if the proposed tool is sensitive enough to distinguish characteristic patterns of brain atrophy in various dementia types.

The DR segmentation algorithm relies on the nearest neighbour search (NNS). Each voxel of the DR is tagged with a label that identifies the nearest MAPER brain

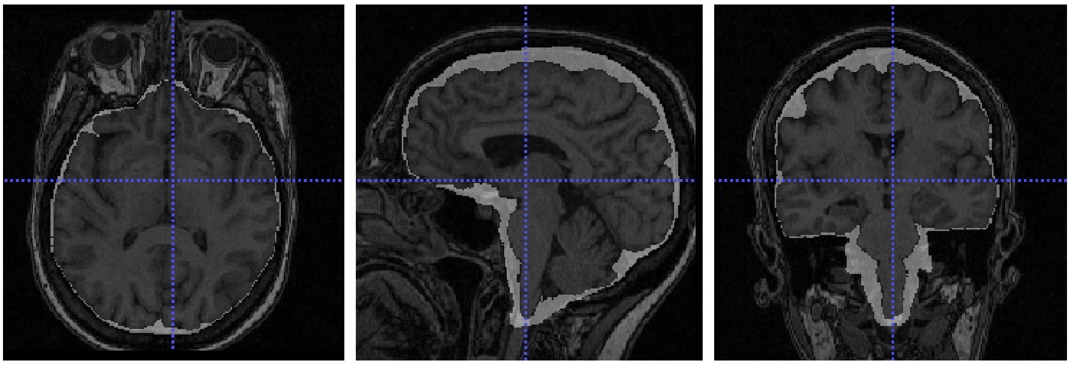

Figure 3.1: A sample DR mask; axial, sagittal and coronal view.

region. A direct approach to the problem would be to use a brute-force search, which involves calculation of the distance between each DR voxel and all voxels belonging to the MAPER segmentation, finding a pair with the shortest distance and tagging the DR voxel with the corresponding MAPER label. This inefficient procedure would be impractical to perform on the images studied here. Several approaches were explored to decrease computation time of the segmentation. A detailed description of the developed procedures is presented in the following sections.

3.3 Segmentation procedures

3.3.1 Centroid-based segmentation

The first approach explored in the project employed finding one characteristic point for each of the MAPER regions adjacent to the DR. A set of those points was then used to find the nearest neighbour of each DR voxel and label that voxel correspondingly. The characteristic point of a brain region was defined as a centroid of a that part of the brain region, which lies in the immediate neighbourhood of the DR (outer surface of the region). The following procedure was designed to procure the points. A single morphological dilation with a $3 \times 3 \times 3$ cube kernel was applied to DR and a double modal dilation was applied to MAPER segmentation, followed by masking with the pincram brain mask, to ensure that each voxel of the pincram mask has a corresponding MAPER label assigned. The intersections, if present, between the dilated DR mask and the processed MAPER segmentations were found and a centroid was calculated for each intersected volume. The Euclidean distance was used to determine the closest centroid to each voxel in the DR. The procedure is summarized in the following equations:

$$S^i = [(DR \oplus K) \cap (BR^i \oplus K^2) \otimes BM] \tag{3.1}$$

$$R^i_{x,y,z} = C^i_{x,y,z}[S^i] \tag{3.2}$$

$$I = argmin\left\{ \sqrt{(R^i_x - V_x)^2 + (R^i_y - V_y)^2 + (R^i_z - V_z)^2} \right\}, \tag{3.3}$$

S^i is the set of i^{th} region voxels adjacent to the DR,
$R^i_{x,y,z}$ is the point of reference – centroid for each brain region i,
$C^i_{x,y,z}$ is the centroid of the i^{th} region,
K is a 3x3x3 cube kernel,
BR^i is the i^{th} brain region,
BM is the brain mask,
I is the index of the final label of a given DR voxel $V_{x,y,z}$.

3.3.2 MAPER surface-based segmentation

In this approach only MAPER voxels which were adjacent to the DR (outer surface) were considered in the NNS (S^i, equation 3.1) to decrease the number of calculations necessary in the direct approach but to improve the centroid-based segmentation.

3.3.3 Volume partitioning approach

Another segmentation procedure addressed the efficiency problem by partitioning the data set for the NNS task using a 3D k-d tree structure [13, 14]. In this case, all the MAPER voxels were included in the query set to find the nearest neighbour of each DR voxel. Although using a subset derived in equation 3.1 would greatly reduce the number of points in the query set, the gain is outbalanced by the computation time it takes to obtain this subset.

The k-d tree algorithm is a hierarchical approach that divides a data set (parent set) into two equal subsets. Each of the newly created subsets becomes a parent set and is further divided until no more division can be applied. The division of a 3 dimensional voxel set is conducted iteratively over each consecutive dimension x, y, and z. One way of bisecting the parent set is by finding the median value of the voxel coordinates for a given dimension [15]. The algorithm applied in this project uses a canonical sliding midpoint for the data set bisection, which is described in detail in [14]. The nearest neighbour search is conducted by following the tree structure from the root (first bisection plane) to the leaf (nearest voxel), by choosing those consecutive branches (bisection planes) whose values fall closer to the coordinate values of a given DR voxel. The algorithm results in a substantial increase in time efficiency for the nearest neighbour search in a 3 dimensional space. The computation time of the k-d tree algorithm is reported to be $O(logN)$ as opposed to $O(dN)$ in linear search for a fixed number of dimensions, where N is the number of data points and d is the number of dimensions [62, 63].

The kd-tree method may result in some mismatches due to rejecting whole branches whose values in one dimension do not meet the query condition. As a result, some nearest neighbours may be omitted in the search. Nonetheless the algorithm is successfully applied in the field of NNS and clustering, as well as in medical image segmentation [16–18].

3.3.4 Maximum probability atlas-based segmentation

One concern regarding the proximity based DR segmentation is that it may underestimate volumes of certain regions if those regions shrink more relative to their immediate neighbours. Consider two adjacent brain regions and approximate the level of atrophy in each as the shortest distance from their respective surfaces to the cranium d_1 and d_2. If there is a substantial difference between these distances, we can suspect that one of these regions may be affected more in a given dementia type. The current procedure will not account for the difference and the boundary b between the adjoining DR labels will be equidistant from the corresponding two MAPER regions. Such a segmentation will bias the atrophy score by equalizing the true difference between the two considered regions. The problem is visualized in Figure 3.2.

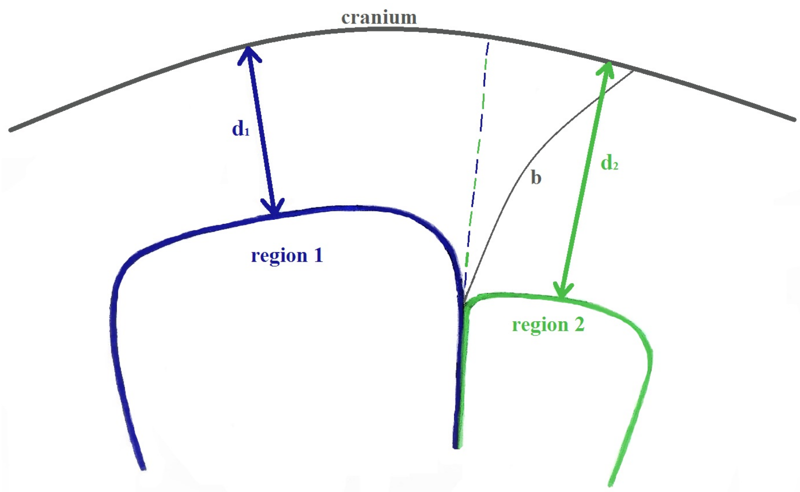

Figure 3.2: A simplified representation of the potential problem with the DR segmentation. The dashed lines represent alleged true segmentation, b represents approximate segmentation obtained with the current approach.

To compensate for varying atrophy levels between brain regions in the DR segmentation, I tested a solution that employed the Hammers_mith maximum probability atlas (MPA) (www.brain-development.org) [49–51], which represents an average brain segmentation into 95 regions in the MNI space. The maximum probability map was registered to each subject's MAPER segmentation with the FSL FLIRT and FNIRT registration tools [58]. Default deformation model parameters were used in the registration process. The MPA is free from atrophy effects between regions, thus using it as a reference anatomical segmentation instead of the original MAPER segmentation allows us to discard the concern of skewing the atrophy distribution.

3.4 Statistical analysis of the data

Volumetric analyses were performed on the data acquired in the segmentation process after normalizing subregions of the DR to the ICV. The following statistical methods were applied to carry out inferences about the collected data. The volumes of each DR label in each subject were expressed as standard scores with the mean and standard deviation for respective labels calculated across healthy controls or another dementia group. The mean and standard deviation of the standardized volumes for each region were then calculated across all subjects belonging to individual dementia groups. The resultant mean was interpreted as an atrophy score of each MAPER region in a given dementia type. The standard deviation was given to provide an auxiliary insight into the standardized volume distribution in a given region. The whole-brain atrophy scores in each dementia group were calculated using a similar procedure applied to the full DR volumes.

Expressing the degree of atrophy with the standard scores is subject to a bias resulting from small sample size or small volumes of the DR subregions. To detect any significant differences between two diagnosis groups, the data were tested against the hypothesis that both the whole brain and regional atrophy in dementia are different from those of the control group (or another dementia group). The tests compared two volume distributions of a given region (or the whole DR) from two diagnosis groups of interest. The Shapiro-Wilk normality test was applied to both groups. Depending on the distribution of the tested set of volumes, a two-sided, two-sample t-test (if both distributions assumed normal) or Mann-Whitney-Wilcoxon test (at least one of the tested distributions assumed not normal or fewer than 3 observations present) was performed at 95% confidence interval. The obtained p-values were corrected for multiple hypotheses testing. The Benjamini-Yekutieli (BY) [64] method was applied in the regional atrophy tests. The whole brain atrophy p-values were adjusted by Holm's [65] procedure.

3.5 Visualization

A cumulative visual representation of the regional discrepancies between the brain and the ICV segmentations observed in participants of respective dementia groups was created. The method highlights portions of the DR which appear in most subjects of a given diagnostic group. These portions are taken to correspond to the cortical regions that show the highest degree of atrophy in this diagnostic group. The following procedure was designed to produce atrophy heat maps (AHM) in MNI space for groups that were sufficiently large (numbers in parenthesis are cross references to the outline shown in Figure 3.3). Coordinates of areas with the highest intensity were used to locate the corresponding anatomical brain region on the MPA.

(1) *ICV extraction* - for each subject's MR scan the ICV was extracted by masking the original scan with the ICV label.

(2) *Spatial normalization* - the resulting image was then spatially normalized to the MNI152 T1 template [55] using FSL FLIRT [56, 57].

(3) *Image summation* - the affine transformation matrix obtained in step (2) was applied to a corresponding DR label. The next step involved summation of obtained images and subsequent intensity normalization. This step highlights the DR areas that are the most prominent in the largest number of subjects. To visualize the effect of dementia in particular parts of the brain, one summation image (AHM) was produced for each of the diagnosis groups, as well as control subjects.

(4) *Control image subtraction* - since the mean age of the patients and healthy controls was over 60 years, the discrepancies in the DR labels may be a result of natural brain shrinking due to aging. To selectively visualize discrepancies that were due to dementia, the AHM obtained from the control group was subtracted from the AHM of respective groups of demented patients.

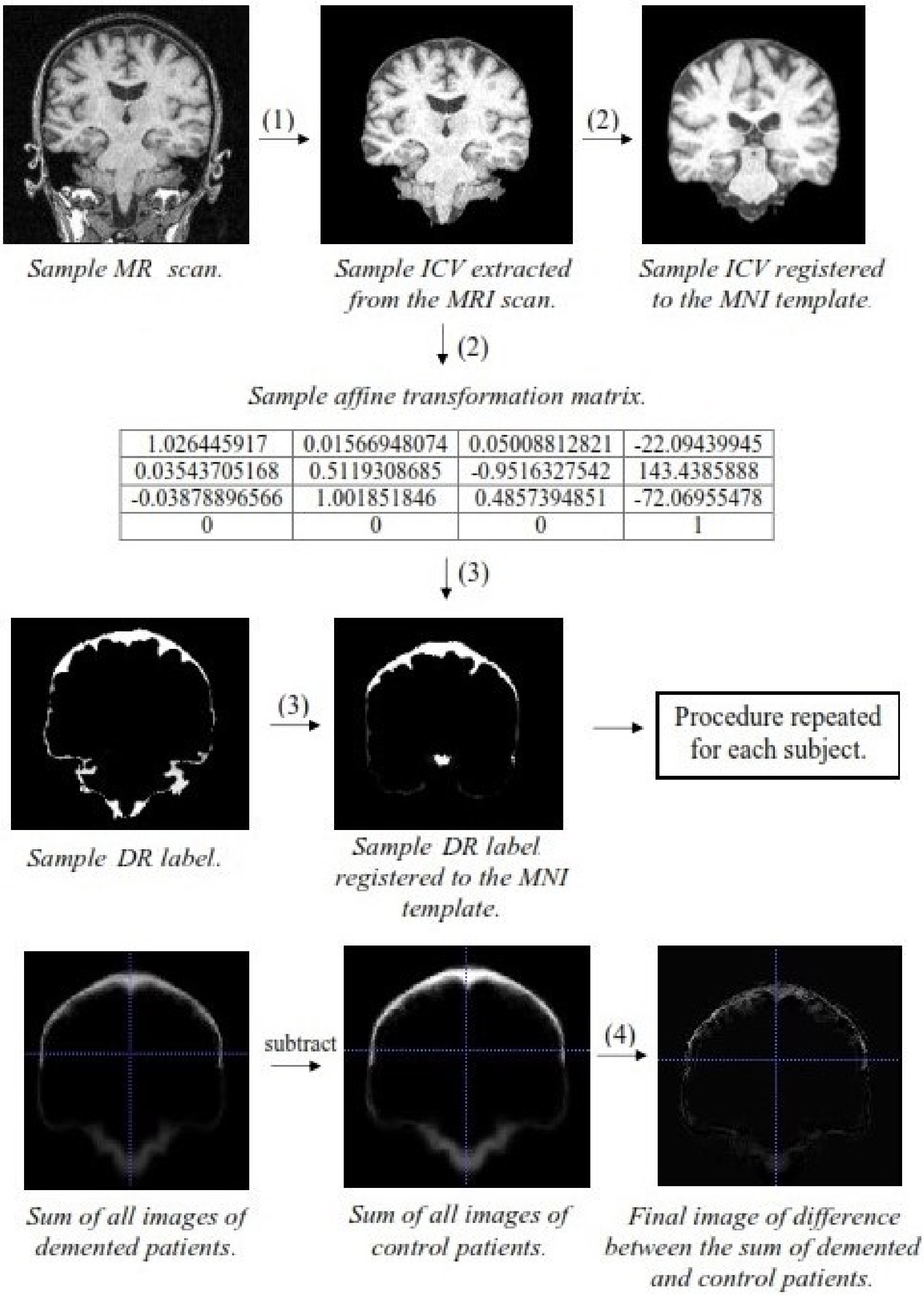

1.026445917	0.01566948074	0.05008812821	-22.09439945
0.03543705168	0.5119308685	-0.9516327542	143.4385888
-0.03878896566	1.001851846	0.4857394851	-72.06955478
0	0	0	1

Figure 3.3: Brain atrophy visualization procedure - sagittal view

4

Segmentation evaluation

Each segmentation algorithm was evaluated on a subset of 62 subjects [61] which had previously been selected from the original MCI database. The evaluation involved visual examination of the resultant DR segmentations overlayed with corresponding MAPER labels. Coherence and continuity between the MAPER and the DR segmented regions as well as computation time were the criteria for assessing a method. The provided computation times are for a Intel Core i7-6700HQ CPU with four processing cores running at 2.60 GHz (Intel Corp., Santa Clara, CA, USA) and 8 GB of RAM.

4.1 Centroid-based segmentation

The centroid-based segmentation was designed to decrease the computation time expected in the brute-force approach by creating only one correspondence point for each DR-adjacent brain label to choose from, while searching for the closest brain region to a given DR voxel. The method examined on a set of 62 subjects showed encouraging results that indicated potential applicability of the approach (Table 4.1). Some inaccuracies, however, became evident during visual examination.

Table 4.1: Preliminary results obtained with the centroid based segmentation: the highest atrophy scores detected in AD.

Region (L - left, R - right)	**Mean z-score**
lateral part of anterior temporal lobe L and R	0.82 and 0.74
middle and inferior part of temporal gyrus L	0.81
supramarginal gyrus in parietal lobe L	0.62
middle part of superior temporal gyrus L	0.61

There exist voxels which lie closer to one MAPER region, but the distance to the reference point of that region is larger than the distance to a reference point of a neighbouring region. Such voxels would be mislabelled by the centroid-based approach, as shown in the Figure 4.1 (top row). The problem mostly concerns relatively large brain regions with a widespread or irregularly-shaped outer surface, whose neighbour regions are smaller and have a more regular outer surface. Even after restricting the number of reference points for the NNS, the intermediate procedures to find the reference points influence the computation time (approximately 25 minutes per subject).

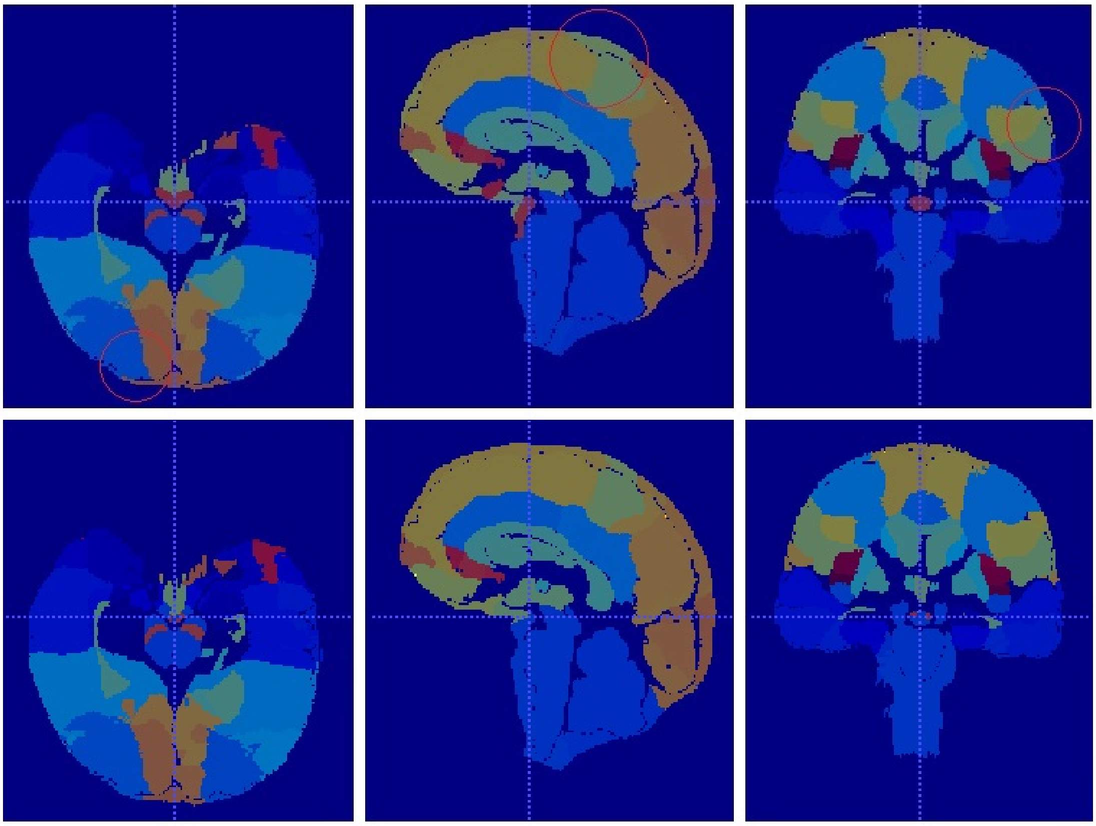

Figure 4.1: The results of centroid based DR segmentation (top row) and a brute-force MAPER proximity approach (bottom row).

4.2 MAPER surface-based segmentation

While the segmentation was improved with this approach (figure 4.1, bottom row), the method was computationally inefficient (taking approximately 30 minutes per subject), and an alternative was developed.

4.3 Volume partitioning approach

The time efficiency of this method greatly improved, decreasing the computation time to approximately 10 seconds per subject. The resultant DR segmentation was highly satisfactory on visual inspection, with no distinct inconsistencies seen (Figure 4.2).

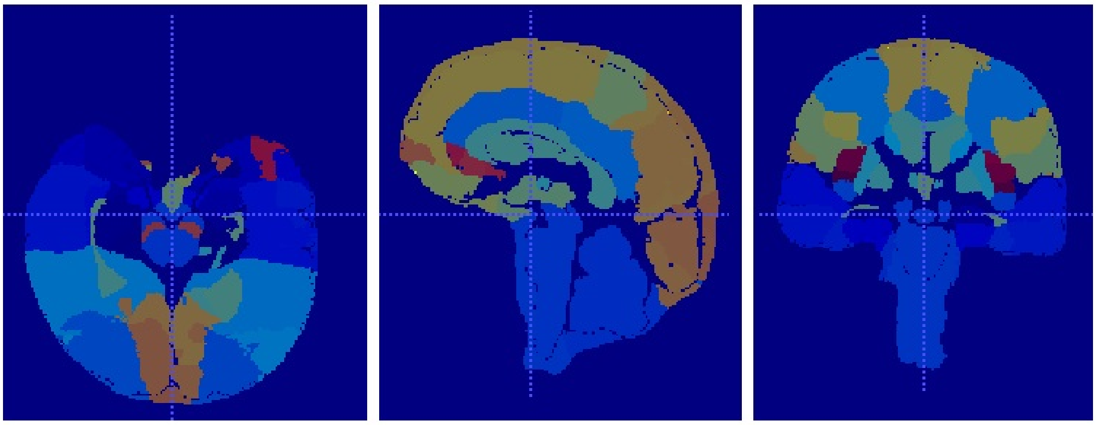

Figure 4.2: The results of DR segmentation using kd-tree volume partitioning.

4.4 Maximum probability atlas-based segmentation

DR segmentation with a linearly registered MPA resulted in an inconsistent region distribution (Figure 4.3, top row) thus a nonlinear registration was attempted. The process of nonlinear registration was performed using default resolution options. It improved the segmentation, but the procedure took approximately 20 minutes per subject.

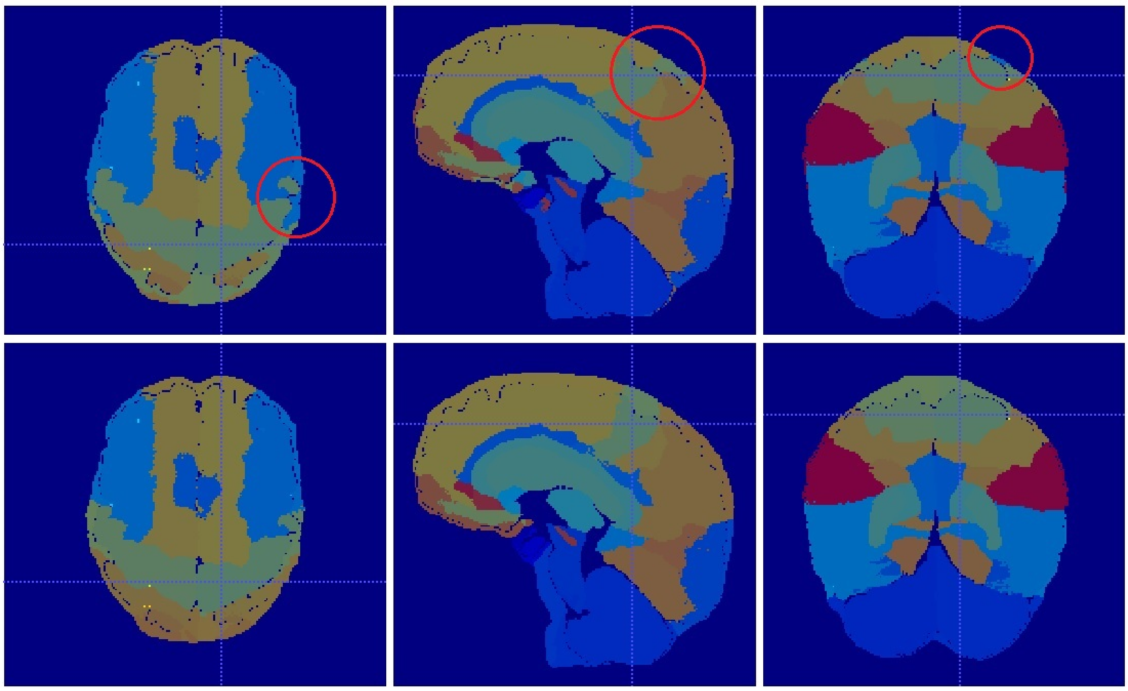

Figure 4.3: The results of DR segmentation using MPA, FLIRT (top row) vs. FNIRT (bottom row).

After visual examination of the segmentations acquired by the described procedures, two of them were deemed feasible: the volume partitioning approach and MPA segmentation. It is difficult, however, to estimate how much each of these segmentations deviate from what would be a "true" segmentation without having a ground truth reference. Visual evaluation alone is not sufficient to determine if there is any genuine benefit in applying the far less time-efficient MPA segmentation. Designing a new algorithm which multiplies the distance from a given DR voxel to the closest MAPER brain region by a weight corresponding to the distance between that region and the cranium may further improve the segmentation. The potential advantage of such an approach over volume partitioning or MPA was considered insufficient at this stage of the project to justify the effort of formulating yet another procedure.

5

Results

5.1 Statistical analysis of the data

This section contains results obtained with the volume partitioning approach (Section 3.3.3) using original MAPER segmentations. The outcome of the whole brain atrophy estimation in each examined dementia type is shown in Table 2.1. The table contains two columns of p-values. The first one contains adjusted p-values for the original classification of the patients (VaD and Mix separately, OC). The second column contains results calculated for Mix and VaD groups combined (MVD).

Table 5.1: The results of whole brain atrophy scores and respective p-values for each dementia group vs. controls.

Dementia group	**Mean z-score**	**SD**	**p-value**^{OC}	**p-value**^{MVD}
FTD	1.66	1.73	1	1
Mix	0.86	0.91	0.003	-
AD	0.83	1.06	0.001	0.001
LBD	0.82	-	1	1
MVD	0.80	0.87	-	0.002
PPA	0.74	-	1	1
VaD	0.68	0.81	0.121	-
NUD	0.65	1.19	0.103	0.091
MCI	0.43	0.92	0.104	0.091
SCI	0.15	1.05	1	1
ND	-0.23	0.75	1	1
Mix FTD/VaD	-0.44	-	1	1

The results of DR subregion volumes analysis for each dementia group versus the control group is presented below (Table 5.2 - 5.9). The data consist of means and standard deviations (SD) of the DR volume z-scores of each region in a given dementia group, and results of testing against the hypothesis that the DR volume distribution of each region in a given demented group is different from the corresponding distribution in the control group. The results contain the analysis of Mix, VaD as separate dementia groups as well as combined. The Tables 5.2 - 5.9 show results for groups containing more than 3 subjects, while Tables 5.10 and 5.11 show the results for groups with only one or 3 subjects. Hypothesis testing is not conducted for these groups.

Table 5.2: AD vs. the control group.

AD, n = 64				
Mean z-score	**SD**	**Region (L - left, R - right)**	**Adjusted p-value**	
0.99	1.55	superior temporal gyrus middle part L	0.023	p-value < 0.05
0.93	1.59	cuneus R	0.023	
0.86	1.3	angular gyrus L	0.023	
0.76	1.03	inferior frontal gyrus R	0.024	
0.75	1.04	third ventricle	0.019	
0.69	1.01	posterior orbital gyrus R	0.027	
0.69	1.18	postcentral gyrus L	0.033	
50.36	71.36	insula anterior short gyrus R	1	p-value > 0.05
13.18	21.3	subcallosal area R	0.965	
3.98	9.38	subcallosal area L	0.574	
0.97	1.86	fusiform gyrus L	0.15	
0.93	1.72	precentral gyrus L	0.178	
0.89	1.39	middle and inferior temporal gyrus R	0.059	
0.87	3.32	insula anterior short gyrus L	1	
0.83	1.59	inferior frontal gyrus L	0.111	
0.75	1.54	posterior temporal lobe L	0.178	
0.75	2.32	insula anterior inferior cortex L	1	
0.74	1.43	superior temporal gyrus anterior part L	0.111	
0.73	1.93	middle and inferior temporal gyrus L	0.574	
0.68	1.61	cuneus L	0.111	
0.64	1.3	postcentral gyrus R	0.114	
0.62	1.08	supramarginal gyrus R	0.064	
0.62	1.04	lateral orbital gyrus R	0.053	
0.61	2.89	substantia nigra L	1	
0.61	1.29	posterior temporal lobe R	0.204	
0.59	1.36	precentral gyrus R	0.2	
0.59	2.12	anterior temporal lobe lateral part L	1	
0.59	1.06	lateral orbital gyrus L	0.053	
0.59	1.16	lateral remainder occipital lobe R	0.053	
0.58	1.17	medial orbital gyrus R	0.178	
0.57	1.9	lingual gyrus L	1	
0.57	1.22	lingual gyrus R	0.178	
0.54	1.23	superior parietal gyrus R	0.178	
0.54	1.15	angular gyrus R	0.193	
0.51	1.02	superior temporal gyrus anterior part R	0.212	
0.5	1.27	middle frontal gyrus L	0.503	
0.49	1.18	superior frontal gyrus R	0.244	
0.49	1.16	anterior temporal lobe lateral part R	0.212	
0.48	1.33	superior frontal gyrus L	0.643	
0.45	0.99	posterior orbital gyrus L	0.111	
0.43	1.09	lateral remainder occipital lobe L	0.193	
0.43	0.93	supramarginal gyrus L	0.193	
0.42	1.17	superior temporal gyrus middle part R	0.545	
0.4	1.06	parahippocampal and ambient gyrus R	0.503	
0.4	1.3	straight gyrus L	0.622	
0.39	1.45	insula anterior inferior cortex R	1	
0.37	1.11	superior parietal gyrus L	0.5	
0.34	1.12	middle frontal gyrus R	0.721	
0.23	0.76	parahippocampal and ambient gyrus L	0.503	
0.21	0.74	medial orbital gyrus L	0.545	
0.18	1.19	fusiform gyrus R	1	
0.17	0.58	anterior temporal lobe medial part L	0.178	
0.17	0.86	cerebellum L	1	
0.14	1.04	anterior orbital gyrus L	1	
0.13	1.05	cerebellum R	1	
0.12	0.93	anterior orbital gyrus R	1	
0.12	0.55	anterior temporal lobe medial part R	0.503	
0.1	1.55	amygdala R	1	
0.04	1.02	straight gyrus R	1	
0.03	0.89	brainstem excluding substantia nigra	1	
-0.12	1.66	amygdala L	0.587	
-0.55	0.29	substantia nigra R	1	

Table 5.3: Mix vs. the control group.

Mix, n = 31

Mean z-score	SD	Region (L - left, R - right)	Adjusted p-value	
1.27	1.45	middle and inferior temporal gyrus L	0.013	p-value < 0.05
1.18	1.85	inferior frontal gyrus L	0.034	
1.1	1.57	superior temporal gyrus middle part L	0.042	
1.01	1.3	cuneus R	0.034	
1	1.4	posterior orbital gyrus R	0.034	
0.96	1.31	lateral remainder occipital lobe R	0.034	
2.58	6.49	subcallosal area L	1	p-value > 0.05
1.17	2.32	insula anterior inferior cortex L	0.361	
1.06	1.89	insula anterior short gyrus L	1	
1.01	1.74	supramarginal gyrus L	0.064	
0.99	1.52	angular gyrus L	0.055	
0.95	1.37	middle and inferior temporal gyrus R	0.064	
0.94	1.5	superior temporal gyrus anterior part L	0.115	
0.93	1.38	posterior temporal lobe L	0.069	
0.86	1.23	cuneus L	0.057	
0.78	1.79	lateral orbital gyrus L	0.685	
0.77	1.31	lateral remainder occipital lobe L	0.106	
0.76	1.42	inferior frontal gyrus R	0.204	
0.75	1.48	middle frontal gyrus L	0.423	
0.7	1.4	fusiform gyrus L	0.401	
0.69	1.16	precentral gyrus L	0.106	
0.68	1.77	subcallosal area R	1	
0.67	1.54	lingual gyrus L	0.699	
0.62	1.05	postcentral gyrus L	0.106	
0.61	1.1	superior frontal gyrus R	0.292	
0.58	0.83	third ventricle	0.064	
0.58	1.28	lingual gyrus R	0.207	
0.57	1.25	posterior orbital gyrus L	0.149	
0.56	1.23	lateral orbital gyrus R	0.594	
0.55	1.23	superior temporal gyrus middle part R	0.423	
0.51	1.35	medial orbital gyrus R	0.782	
0.49	1.03	superior frontal gyrus L	0.476	
0.46	1.05	angular gyrus R	0.454	
0.45	1.34	insula anterior inferior cortex R	0.423	
0.45	1.47	anterior temporal lobe lateral part L	1	
0.43	1.24	straight gyrus L	0.799	
0.43	1.09	superior temporal gyrus anterior part R	0.732	
0.42	1.1	postcentral gyrus R	0.685	
0.4	0.97	parahippocampal and ambient gyrus R	0.594	
0.4	0.8	posterior temporal lobe R	0.355	
0.36	0.85	medial orbital gyrus L	0.408	
0.32	0.88	supramarginal gyrus R	0.747	
0.32	1.06	superior parietal gyrus R	0.972	
0.3	0.71	cerebellum L	0.527	
0.3	1.09	middle frontal gyrus R	1	
0.3	0.69	anterior temporal lobe medial part R	0.262	
0.29	1.37	anterior orbital gyrus L	1	
0.28	1.04	superior parietal gyrus L	0.854	
0.26	1.14	anterior temporal lobe lateral part R	1	
0.25	0.8	cerebellum R	0.972	
0.23	0.59	anterior temporal lobe medial part L	0.106	
0.21	0.99	anterior orbital gyrus R	1	
0.16	1.4	amygdala R	1	
0.16	0.91	precentral gyrus R	1	
0.09	0.87	parahippocampal and ambient gyrus L	1	
0.08	0.89	substantia nigra R	1	
0.05	1.24	straight gyrus R	1	
0	0.89	brainstem excluding substantia nigra	1	
-0.08	0.95	fusiform gyrus R	1	
-0.13	1.01	amygdala L	1	
-0.14	0.77	substantia nigra L	1	

Table 5.4: VaD vs. the conrol group.

VaD, n =14			
Mean z-score	**SD**	**Region (L - left, R - right)**	**Adjusted p-value**
3.29	6.01	subcallosal area R	1
1.44	1.69	posterior temporal lobe R	0.141
1.31	3.62	substantia nigra L	1
1.24	1.6	superior temporal gyrus middle part R	0.308
1.17	1.94	fusiform gyrus L	0.366
1.1	1.18	middle and inferior temporal gyrus R	0.189
1.02	0.97	third ventricle	0.141
1.02	1.65	inferior frontal gyrus R	0.345
0.96	1.28	lateral orbital gyrus R	0.345
0.93	1.12	inferior frontal gyrus L	0.345
0.93	1.42	lingual gyrus R	0.353
0.92	1.41	brainstem excluding substantia nigra	0.308
0.9	1.34	medial orbital gyrus R	0.423
0.88	2.02	amygdala R	1
0.87	1.81	superior temporal gyrus anterior part R	0.927
0.86	1.32	parahippocampal and ambient gyrus L	0.424
0.85	1.19	amygdala L	0.423
0.82	1.4	middle frontal gyrus L	0.548
0.81	1.28	superior temporal gyrus middle part L	0.366
0.78	1.78	parahippocampal and ambient gyrus R	1
0.73	1.16	cerebellum R	0.578
0.71	0.74	supramarginal gyrus R	0.308
0.7	1.04	lateral orbital gyrus L	0.364
0.69	1.13	middle frontal gyrus R	0.402
0.69	1.38	medial orbital gyrus L	0.582
0.64	0.93	angular gyrus L	0.402
0.59	1.33	superior temporal gyrus anterior part L	1
0.59	0.81	angular gyrus R	0.366
0.55	0.85	cerebellum L	0.423
0.54	1.38	middle and inferior temporal gyrus L	1
0.54	0.79	lateral remainder occipital lobe R	0.345
0.48	1.14	lingual gyrus L	1
0.42	0.96	anterior temporal lobe lateral part R	1
0.42	1.08	supramarginal gyrus L	1
0.37	1.27	fusiform gyrus R	1
0.35	0.8	straight gyrus L	1
0.34	1.08	posterior temporal lobe L	1
0.28	1.1	precentral gyrus L	1
0.27	0.8	lateral remainder occipital lobe L	1
0.27	1.12	posterior orbital gyrus R	1
0.24	0.92	insula anterior inferior cortex L	1
0.22	1.07	cuneus R	1
0.22	0.63	precentral gyrus R	1
0.21	0.79	posterior orbital gyrus L	1
0.19	1.84	anterior orbital gyrus R	1
0.19	0.57	anterior temporal lobe medial part L	0.809
0.19	1.32	insula anterior inferior cortex R	1
0.17	0.58	superior frontal gyrus L	1
0.15	0.83	postcentral gyrus L	1
0.13	1.58	substantia nigra R	1
0.13	0.82	superior parietal gyrus R	1
0.12	0.59	superior frontal gyrus R	1
0.12	1.05	anterior orbital gyrus L	1
0.1	0.79	insula anterior short gyrus L	1
0.1	0.78	postcentral gyrus R	1
0.07	0.97	anterior temporal lobe medial part R	1
0.02	1.15	anterior temporal lobe lateral part L	1
-0.02	0.91	subcallosal area L	1
-0.02	0.67	cuneus L	1
-0.05	0.95	straight gyrus R	1
-0.11	0.83	superior parietal gyrus L	1

p-value > 0.05

Table 5.5: MVD vs. the control group

		MVD, n = 46		
Mean z-score	**SD**	**Region (L - left, R - right)**	**Adjusted p-value**	
1.1	1.65	inferior frontal gyrus L	0.013	p-value < 0.05
1.05	1.45	middle and inferior temporal gyrus L	0.013	
1.01	1.48	superior temporal gyrus middle part L	0.016	
1	1.3	middle and inferior temporal gyrus R	0.014	
0.88	1.37	angular gyrus L	0.023	
0.83	1.18	lateral remainder occipital lobe R	0.013	
0.71	0.89	third ventricle	0.013	
1.82	5.54	subcallosal area L	1	p-value > 0.05
1.21	2.77	subcallosal area R	1	
0.9	2.05	insula anterior inferior cortex L	0.422	
0.84	1.58	fusiform gyrus L	0.123	
0.83	1.48	inferior frontal gyrus R	0.076	
0.83	1.44	superior temporal gyrus anterior part L	0.119	
0.83	1.58	supramarginal gyrus L	0.076	
0.78	1.35	posterior orbital gyrus R	0.06	
0.77	1.28	cuneus R	0.086	
0.77	1.44	middle frontal gyrus L	0.156	
0.76	1.37	superior temporal gyrus middle part R	0.111	
0.76	1.59	lateral orbital gyrus L	0.17	
0.75	1.31	posterior temporal lobe L	0.119	
0.72	1.23	posterior temporal lobe R	0.06	
0.72	1.62	insula anterior short gyrus L	1	
0.68	1.32	lingual gyrus R	0.076	
0.68	1.25	lateral orbital gyrus R	0.156	
0.63	1.34	medial orbital gyrus R	0.248	
0.62	1.19	lateral remainder occipital lobe L	0.111	
0.61	1.42	lingual gyrus L	0.518	
0.59	1.15	cuneus L	0.17	
0.57	1.14	precentral gyrus L	0.17	
0.56	1.35	superior temporal gyrus anterior part R	0.343	
0.52	1.27	parahippocampal and ambient gyrus R	0.343	
0.5	0.98	angular gyrus R	0.144	
0.48	1	postcentral gyrus L	0.156	
0.46	1.14	posterior orbital gyrus L	0.144	
0.46	1.04	medial orbital gyrus L	0.156	
0.46	0.99	superior frontal gyrus R	0.244	
0.44	0.85	supramarginal gyrus R	0.161	
0.42	1.1	middle frontal gyrus R	0.334	
0.4	1.12	straight gyrus L	0.445	
0.39	0.92	superior frontal gyrus L	0.422	
0.39	0.94	cerebellum R	0.37	
0.39	2.2	substantia nigra L	1	
0.38	1.62	amygdala R	1	
0.38	0.76	cerebellum L	0.17	
0.37	1.33	insula anterior inferior cortex R	0.754	
0.33	1.02	postcentral gyrus R	0.727	
0.32	1.08	parahippocampal and ambient gyrus L	1	
0.32	1.38	anterior temporal lobe lateral part L	1	
0.31	1.08	anterior temporal lobe lateral part R	0.841	
0.28	1.14	brainstem excluding substantia nigra	1	
0.26	0.99	superior parietal gyrus R	1	
0.24	1.27	anterior orbital gyrus L	1	
0.23	0.78	anterior temporal lobe medial part R	0.545	
0.22	0.58	anterior temporal lobe medial part L	0.076	
0.21	1.28	anterior orbital gyrus R	1	
0.19	1.16	amygdala L	1	
0.18	0.83	precentral gyrus R	1	
0.16	0.99	superior parietal gyrus L	1	
0.1	1.04	substantia nigra R	1	
0.06	1.06	fusiform gyrus R	1	
0.02	1.15	straight gyrus R	1	

Table 5.6: NUD vs. the control group.

		NUD, n = 37	
Mean z-score	**SD**	**Region (L - left, R - right)**	**Adjusted p-value**
3.17	5.98	subcallosal area L	0.501
1.31	3.12	insula anterior short gyrus L	1
1.24	2.21	inferior frontal gyrus L	0.142
1.22	2.15	superior temporal gyrus anterior part L	0.142
1.12	3.18	insula anterior inferior cortex L	1
1.1	1.84	superior temporal gyrus middle part L	0.142
1.01	2	inferior frontal gyrus R	0.152
0.99	1.96	middle and inferior temporal gyrus L	0.304
0.94	1.64	superior temporal gyrus anterior part R	0.142
0.91	2.37	middle frontal gyrus L	0.783
0.87	1.33	parahippocampal and ambient gyrus R	0.142
0.86	1.51	medial orbital gyrus R	0.142
0.86	1.49	lateral orbital gyrus R	0.142
0.85		insula anterior short gyrus R	0.29
0.81	1.54	fusiform gyrus L	0.32
0.75	1.59	posterior orbital gyrus R	0.18
0.75	1.28	posterior temporal lobe R	1
0.74	2.37	substantia nigra R	0.142
0.74	1.27	parahippocampal and ambient gyrus L	1
0.71	3.32	subcallosal area R	0.142
0.69	1.38	posterior orbital gyrus L	0.783
0.68	1.72	superior temporal gyrus middle part R	0.595
0.65	1.37	middle and inferior temporal gyrus R	0.451
0.58	1.31	straight gyrus L	0.142
0.57	1.09	medial orbital gyrus L	0.626
0.57	1.31	fusiform gyrus R	1
0.55	1.55	lateral orbital gyrus L	0.375
0.54	1.42	cuneus R	0.269
0.52	1.07	third ventricle	1
0.51	1.41	supramarginal gyrus L	1
0.49	1.32	supramarginal gyrus R	0.823
0.48	1.26	brainstem excluding substantia nigra	1
0.46	1.48	lingual gyrus R	0.783
0.46	1.35	angular gyrus R	1
0.42	1.42	middle frontal gyrus R	1
0.42	1.13	cuneus L	1
0.41	1.25	anterior temporal lobe lateral part R	1
0.4	1.29	superior parietal gyrus R	1
0.39	1.07	postcentral gyrus L	0.594
0.37	0.81	cerebellum R	1
0.37	1.31	posterior temporal lobe L	1
0.36	1.22	anterior orbital gyrus L	1
0.35	1.32	precentral gyrus R	1
0.34	1.47	anterior temporal lobe lateral part L	1
0.33	1.21	lingual gyrus L	1
0.29	1.14	angular gyrus L	0.142
0.25	0.69	anterior temporal lobe medial part L	1
0.24	1.34	postcentral gyrus R	1
0.24	1.19	straight gyrus R	1
0.24	0.89	cerebellum L	1
0.21	1.38	precentral gyrus L	1
0.21	1.09	superior frontal gyrus R	1
0.21	1.65	insula anterior inferior cortex R	1
0.2	0.77	anterior temporal lobe medial part R	1
0.2	1	anterior orbital gyrus R	1
0.19	1.35	lateral remainder occipital lobe R	1
0.14	1.17	superior parietal gyrus L	1
0.14	1.14	superior frontal gyrus L	1
0.09	1.44	substantia nigra L	1
0.06	1.27	amygdala R	1
-0.02	1.05	lateral remainder occipital lobe L	1

p-value > 0.05

Table 5.7: MCI vs. the control group

MCI, n = 160			
Mean z-score	**SD**	**Region (L - left, R - right)**	**Adjusted p-value**
6.01	4.49	insula anterior short gyrus R	1
2.55	6.05	subcallosal area R	1
1.29	3.79	subcallosal area L	1
0.68	1.34	middle and inferior temporal gyrus L	0.533
0.61	1.22	cuneus R	0.533
0.58	1.58	precentral gyrus L	1
0.53	1.22	middle and inferior temporal gyrus R	0.916
0.51	1.38	superior temporal gyrus middle part L	0.916
0.5	1.29	medial orbital gyrus R	0.916
0.48	1.37	lingual gyrus R	0.916
0.48	1.37	fusiform gyrus L	0.916
0.47	1.41	posterior orbital gyrus R	0.916
0.43	1.36	posterior temporal lobe L	1
0.43	1.09	inferior frontal gyrus L	0.916
0.4	1.33	angular gyrus L	1
0.4	1.14	inferior frontal gyrus R	0.916
0.38	1.37	lateral orbital gyrus L	1
0.38	1.1	superior temporal gyrus anterior part L	0.916
0.38	1.04	supramarginal gyrus L	0.916
0.38	1.13	middle frontal gyrus L	1
0.36	1.1	superior parietal gyrus R	0.916
0.34	1.13	postcentral gyrus L	0.934
0.32	1.21	lateral remainder occipital lobe R	1
0.31	1.22	angular gyrus R	1
0.31	1.15	cuneus L	1
0.31	1.18	posterior temporal lobe R	1
0.29	0.91	third ventricle	0.916
0.27	1.85	substantia nigra L	1
0.26	1.12	supramarginal gyrus R	1
0.26	0.99	superior temporal gyrus anterior part R	1
0.26	0.97	superior frontal gyrus R	1
0.25	1.45	anterior temporal lobe lateral part L	1
0.25	0.95	superior frontal gyrus L	1
0.25	1.13	posterior orbital gyrus L	0.916
0.23	1.58	insula anterior inferior cortex L	1
0.23	1.14	anterior temporal lobe lateral part R	1
0.2	1.1	lateral orbital gyrus R	1
0.2	0.9	medial orbital gyrus L	1
0.2	0.85	cerebellum L	1
0.2	1.09	superior parietal gyrus L	1
0.18	1.05	cerebellum R	1
0.17	1.28	insula anterior inferior cortex R	1
0.16	1.39	lingual gyrus L	1
0.16	1.05	postcentral gyrus R	1
0.15	0.97	parahippocampal and ambient gyrus R	1
0.15	1.11	straight gyrus L	1
0.14	1.14	lateral remainder occipital lobe L	1
0.14	0.84	parahippocampal and ambient gyrus L	1
0.09	1.06	superior temporal gyrus middle part R	1
0.09	0.98	precentral gyrus R	1
0.06	0.9	middle frontal gyrus R	1
0.05	0.59	anterior temporal lobe medial part L	1
0.05	1	insula anterior short gyrus L	1
0.04	1.44	amygdala L	1
0.04	0.67	anterior temporal lobe medial part R	1
0.03	1.23	anterior orbital gyrus L	1
0.03	1.66	amygdala R	1
0.02	1.13	fusiform gyrus R	1
-0.01	1.08	brainstem excluding substantia nigra	1
-0.09	0.87	anterior orbital gyrus R	1
-0.11	1.24	substantia nigra R	1
-0.19	0.97	straight gyrus R	1

p-value > 0.05

Table 5.8: SCI vs. the control group

SCI, n =137

Mean z-score	**SD**	**Region (L - left, R - right)**	**Adjusted p-value**
2.46	3.77	insula anterior short gyrus R	1
0.89	2.44	subcallosal area R	1
0.74	2.84	substantia nigra L	1
0.58	1.92	subcallosal area L	1
0.45	1.26	middle and inferior temporal gyrus L	1
0.44	1.52	precentral gyrus L	1
0.4	0.93	middle and inferior temporal gyrus R	1
0.36	1.12	postcentral gyrus L	1
0.35	1.49	fusiform gyrus L	1
0.29	1.46	angular gyrus L	1
0.29	1.49	cuneus R	1
0.27	1.25	posterior orbital gyrus R	1
0.26	1.19	inferior frontal gyrus R	1
0.26	1.2	medial orbital gyrus R	1
0.25	1.27	lingual gyrus R	1
0.22	1.18	angular gyrus R	1
0.22	1.17	insula anterior inferior cortex L	1
0.19	1.23	supramarginal gyrus L	1
0.19	1.08	inferior frontal gyrus L	1
0.18	1.04	superior temporal gyrus anterior part L	1
0.18	1.05	lateral orbital gyrus R	1
0.16	0.98	straight gyrus L	1
0.16	1.42	cuneus L	1
0.16	1.14	superior temporal gyrus middle part L	1
0.15	1.13	superior parietal gyrus R	1
0.15	1.26	middle frontal gyrus L	1
0.13	1.05	superior frontal gyrus R	1
0.13	0.99	insula anterior short gyrus L	1
0.12	0.96	supramarginal gyrus R	1
0.12	0.86	third ventricle	1
0.11	1.09	postcentral gyrus R	1
0.1	0.87	superior temporal gyrus anterior part R	1
0.1	0.97	lateral orbital gyrus L	1
0.1	1.1	precentral gyrus R	1
0.08	0.97	medial orbital gyrus L	1
0.07	1.02	posterior orbital gyrus L	1
0.06	1.11	posterior temporal lobe L	1
0.05	1.21	lateral remainder occipital lobe R	1
0.05	0.89	parahippocampal and ambient gyrus R	1
0.04	1.05	posterior temporal lobe R	1
0.03	1.04	superior frontal gyrus L	1
0.03	1.31	amygdala R	1
0	1.14	middle frontal gyrus R	1
-0.01	0.92	cerebellum L	1
-0.01	1.06	amygdala L	1
-0.02	1	insula anterior inferior cortex R	1
-0.03	1.06	superior parietal gyrus L	1
-0.03	0.96	cerebellum R	1
-0.04	0.54	anterior temporal lobe medial part R	1
-0.05	0.85	anterior temporal lobe lateral part R	1
-0.05	1.26	lingual gyrus L	1
-0.06	0.43	anterior temporal lobe medial part L	1
-0.06	0.76	parahippocampal and ambient gyrus L	1
-0.08	1.1	anterior temporal lobe lateral part L	1
-0.09	1.05	brainstem excluding substantia nigra	1
-0.11	1.12	lateral remainder occipital lobe L	1
-0.14	0.93	straight gyrus R	1
-0.15	1	anterior orbital gyrus L	1
-0.16	1.05	superior temporal gyrus middle part R	1
-0.18	1.06	fusiform gyrus R	1
-0.18	0.79	anterior orbital gyrus R	1
-0.21	1.02	substantia nigra R	1

p-value > 0.05

Table 5.9: ND vs. the control group.

		ND, n = 14		
Mean z-score	**SD**	**Region (L - left, R - right)**	**Adjusted p-value**	
3.5	-	subcallosal area L	1	p-value > 0.05
3.33	0.74	substantia nigra L	1	
1.57	2.2	insula anterior short gyrus L	1	
0.87	2.93	amygdala R	1	
0.51	1.37	insula anterior inferior cortex L	1	
0.4	1.12	postcentral gyrus R	1	
0.38	1.03	middle and inferior temporal gyrus R	1	
0.38	1.21	supramarginal gyrus L	1	
0.36	1.16	postcentral gyrus L	1	
0.34	0.93	third ventricle	1	
0.33	0.91	posterior orbital gyrus R	1	
0.26	1.38	precentral gyrus L	1	
0.26	0.92	straight gyrus L	1	
0.26	1.1	cuneus R	1	
0.25	0.99	medial orbital gyrus L	1	
0.24	0.91	lateral orbital gyrus L	1	
0.2	0.84	parahippocampal and ambient gyrus R	1	
0.2	1.39	angular gyrus L	1	
0.17	1.25	angular gyrus R	1	
0.16	1.12	superior temporal gyrus middle part L	1	
0.14	0.41	anterior temporal lobe medial part R	1	
0.13	0.96	medial orbital gyrus R	1	
0.07	0.9	superior parietal gyrus L	1	
0.05	1.12	insula anterior inferior cortex R	1	
0.03	0.71	anterior orbital gyrus R	1	
0	1.16	middle frontal gyrus L	1	
-0.01	0.79	parahippocampal and ambient gyrus L	1	
-0.02	1.06	anterior temporal lobe lateral part R	1	
-0.06	0.99	superior parietal gyrus R	1	
-0.06	0.79	precentral gyrus R	1	
-0.07	0.91	fusiform gyrus L	1	
-0.09	0.61	lateral orbital gyrus R	1	
-0.09	1.29	middle and inferior temporal gyrus L	1	
-0.1	0.74	lingual gyrus R	1	
-0.13	0.74	inferior frontal gyrus L	1	
-0.14	0.72	straight gyrus R	1	
-0.15	0.64	superior temporal gyrus anterior part L	1	
-0.16	0.57	middle frontal gyrus R	1	
-0.17	1.04	anterior orbital gyrus L	1	
-0.2	0.75	superior frontal gyrus L	1	
-0.2	0.78	lateral remainder occipital lobe R	1	
-0.22	0.98	supramarginal gyrus R	1	
-0.24	0.27	anterior temporal lobe medial part L	1	
-0.25	1.36	anterior temporal lobe lateral part L	1	
-0.26	0.52	posterior orbital gyrus L	1	
-0.26	0.62	superior frontal gyrus R	1	
-0.28	0.64	superior temporal gyrus middle part R	1	
-0.28	0.59	superior temporal gyrus anterior part R	1	
-0.29	0.65	inferior frontal gyrus R	1	
-0.3	0.96	brainstem excluding substantia nigra	1	
-0.33	0.67	cuneus L	1	
-0.4	1.1	fusiform gyrus R	1	
-0.4	0.74	amygdala L	1	
-0.4	0.64	lateral remainder occipital lobe L	1	
-0.5	0.35	substantia nigra R	1	
-0.61	0.75	cerebellum L	1	
-0.62	0.81	posterior temporal lobe R	1	
-0.63	0.69	posterior temporal lobe L	1	
-0.66	0.79	cerebellum R	1	

Table 5.10: FTD and PPA vs. the control

FTD, n = 3		**PPA, n = 1**	
Mean z-score	**Region (L -left, R - right)**	**Mean z-score**	**Region (L -left, R - right)**
3.85	fusiform gyrus L	4.45	superior temporal gyrus middle part L
3.20	middle frontal gyrus L	3.33	posterior temporal lobe L
2.75	middle frontal gyrus R	3.06	anterior orbital gyrus L
2.56	inferior frontal gyrus L	3.05	anterior temporal lobe lateral part L
2.49	inferior frontal gyrus R	2.73	third ventricle
2.16	lateral orbital gyrus R	2.56	subcallosal area L
2.14	fusiform gyrus R	1.80	middle and inferior temporal gyrus L
2.01	superior frontal gyrus L	1.73	lateral remainder occipital lobe L
1.91	lateral orbital gyrus L	1.61	angular gyrus L
1.90	superior frontal gyrus R	1.43	parahippocampal and ambient gyrus R
1.89	middle and inferior temporal gyrus R	1.38	parahippocampal and ambient gyrus L
1.60	precentral gyrus L	1.27	lingual gyrus R
1.55	straight gyrus L	1.25	cerebellum R
1.48	insula anterior inferior cortex L	1.07	supramarginal gyrus L
1.39	superior temporal gyrus anterior part R	0.92	substantia nigra R
1.20	middle and inferior temporal gyrus L	0.91	anterior temporal lobe lateral part R
1.20	anterior orbital gyrus R	0.90	superior frontal gyrus R
1.16	posterior temporal lobe L	0.89	lateral orbital gyrus L
1.15	superior temporal gyrus anterior part L	0.86	lateral remainder occipital lobe R
1.14	superior temporal gyrus middle part L	0.85	middle frontal gyrus L
1.00	straight gyrus R	0.85	posterior temporal lobe R
0.86	postcentral gyrus L	0.68	superior frontal gyrus L
0.75	anterior temporal lobe lateral part R	0.67	postcentral gyrus L
0.71	amygdala R	0.64	anterior orbital gyrus R
0.70	medial orbital gyrus L	0.58	inferior frontal gyrus L
0.63	posterior temporal lobe R	0.56	fusiform gyrus R
0.62	cuneus R	0.53	brainstem excluding substantia nigra
0.61	posterior orbital gyrus R	0.51	lingual gyrus L
0.61	anterior temporal lobe medial part R	0.47	lateral orbital gyrus R
0.58	postcentral gyrus R	0.38	superior temporal gyrus middle part R
0.57	anterior temporal lobe medial part L	0.35	middle frontal gyrus R
0.53	anterior temporal lobe lateral part L	0.35	cerebellum L
0.50	cuneus L	0.33	fusiform gyrus L
0.45	superior temporal gyrus middle part R	0.23	middle and inferior temporal gyrus R
0.38	supramarginal gyrus R	0.19	medial orbital gyrus R
0.38	parahippocampal and ambient gyrus L	0.17	precentral gyrus L
0.36	parahippocampal and ambient gyrus R	0.15	superior temporal gyrus anterior part L
0.34	precentral gyrus R	-0.01	cuneus R
0.33	angular gyrus R	-0.05	postcentral gyrus R
0.30	medial orbital gyrus R	-0.09	cuneus L
0.23	superior parietal gyrus L	-0.16	anterior temporal lobe medial part L
0.21	brainstem excluding substantia nigra	-0.21	anterior temporal lobe medial part R
0.21	insula anterior inferior cortex R	-0.35	medial orbital gyrus L
0.19	cerebellum L	-0.39	supramarginal gyrus R
0.16	superior parietal gyrus R	-0.50	superior parietal gyrus R
0.12	cerebellum R	-0.52	posterior orbital gyrus R
0.11	third ventricle	-0.62	inferior frontal gyrus R
0.10	lingual gyrus R	-0.64	posterior orbital gyrus L
-0.01	insula anterior short gyrus L	-0.70	precentral gyrus R
-0.13	anterior orbital gyrus L	-0.75	angular gyrus R
-0.15	lateral remainder occipital lobe L	-0.77	insula anterior inferior cortex R
-0.17	supramarginal gyrus L	-0.77	superior temporal gyrus anterior part R
-0.18	lingual gyrus L	-0.85	superior parietal gyrus L
-0.21	amygdala L	-0.85	amygdala R
-0.29	posterior orbital gyrus L	-0.87	insula anterior inferior cortex L
-0.31	lateral remainder occipital lobe R	-1.02	straight gyrus L
		-1.54	amygdala L

Table 5.11: LBD and Mix FTD/VaD vs. the control group

LBD, n = 1		**Mix FTD/VaD, n = 1**	
Mean z-score	**Region (L -left, R - right)**	**Mean z-score**	**Region (L -left, R - right)**
4.11	superior temporal gyrus middle part L	8.20	insula anterior short gyrus R
2.62	inferior frontal gyrus L	3.56	anterior orbital gyrus R
2.44	superior temporal gyrus anterior part R	3.04	anterior orbital gyrus L
2.00	superior temporal gyrus middle part R	2.94	posterior orbital gyrus L
1.92	angular gyrus L	2.81	posterior temporal lobe R
1.87	subcallosal area R	2.69	medial orbital gyrus R
1.86	fusiform gyrus R	2.68	amygdala L
1.86	supramarginal gyrus R	2.31	middle and inferior temporal gyrus R
1.84	postcentral gyrus R	2.30	substantia nigra L
1.60	postcentral gyrus L	2.30	posterior orbital gyrus R
1.57	inferior frontal gyrus R	1.94	lateral orbital gyrus R
1.50	middle frontal gyrus L	1.32	third ventricle
1.47	cuneus R	1.13	superior temporal gyrus anterior part R
1.36	middle frontal gyrus R	1.07	medial orbital gyrus L
1.33	precentral gyrus R	1.02	middle frontal gyrus L
1.27	lateral orbital gyrus R	0.96	anterior temporal lobe medial part R
1.25	lingual gyrus R	0.90	anterior temporal lobe medial part L
1.16	posterior orbital gyrus R	0.78	middle and inferior temporal gyrus L
1.12	superior temporal gyrus anterior part L	0.77	straight gyrus L
1.05	straight gyrus R	0.67	posterior temporal lobe L
0.91	superior parietal gyrus L	0.64	cuneus R
0.90	anterior temporal lobe lateral part R	0.61	inferior frontal gyrus R
0.88	anterior temporal lobe lateral part L	0.57	lateral orbital gyrus L
0.85	lateral remainder occipital lobe R	0.52	amygdala R
0.82	parahippocampal and ambient gyrus R	0.51	superior temporal gyrus anterior part L
0.78	superior parietal gyrus R	0.47	anterior temporal lobe lateral part R
0.74	brainstem excluding substantia nigra	0.43	lateral remainder occipital lobe L
0.55	precentral gyrus L	0.40	lateral remainder occipital lobe R
0.51	anterior orbital gyrus L	0.38	middle frontal gyrus R
0.50	medial orbital gyrus R	0.37	inferior frontal gyrus L
0.45	anterior orbital gyrus R	0.31	angular gyrus R
0.44	supramarginal gyrus L	0.20	parahippocampal and ambient gyrus L
0.44	insula anterior inferior cortex R	0.07	cuneus L
0.36	straight gyrus L	0.06	angular gyrus L
0.34	lateral remainder occipital lobe L	-0.03	superior frontal gyrus R
0.32	cuneus L	-0.10	superior temporal gyrus middle part R
0.26	anterior temporal lobe medial part R	-0.33	brainstem excluding substantia nigra
0.07	third ventricle	-0.35	straight gyrus R
0.035	insula anterior inferior cortex L	-0.37	fusiform gyrus R
0.00	fusiform gyrus L	-0.42	superior frontal gyrus L
-0.04	parahippocampal and ambient gyrus L	-0.43	supramarginal gyrus R
-0.08	medial orbital gyrus L	-0.51	supramarginal gyrus L
-0.17	anterior temporal lobe medial part L	-0.51	parahippocampal and ambient gyrus R
-0.19	superior frontal gyrus L	-0.64	anterior temporal lobe lateral part L
-0.27	posterior orbital gyrus L	-0.64	insula anterior inferior cortex L
-0.30	lateral orbital gyrus L	-0.65	lingual gyrus L
-0.52	superior frontal gyrus R	-0.74	cerebellum R
-0.56	middle and inferior temporal gyrus L	-0.78	insula anterior inferior cortex R
-0.59	cerebellum L	-0.81	superior temporal gyrus middle part L
-0.79	posterior temporal lobe R	-0.91	precentral gyrus R
-0.79	lingual gyrus L	-0.99	cerebellum L
-0.85	middle and inferior temporal gyrus R	-1.10	precentral gyrus L
-0.91	subcallosal area L	-1.10	postcentral gyrus L
-0.93	amygdala L	-1.13	fusiform gyrus L
-0.93	posterior temporal lobe L	-1.36	superior parietal gyrus R
-1.00	amygdala R	-1.48	lingual gyrus R
-1.08	cerebellum R	-1.61	superior parietal gyrus L

Testing for differences between two dementia groups was conducted for the following pairs: Mix vs. AD, Mix vs. VaD, Ad vs. VaD and AD vs MVD. The choice of these pairs is dictated by a particular interest in finding atrophy locations that might help to differentiate between given two dementia types. The results did not show any significantly differing regions in any of the examined pairs.

5.2 Visualization

The following figures contain the most atrophied areas found by the proposed visualization method. Each figure contains 3 sections: axial, sagittal and coronal (from left to right). Captions include identification of the indicated left (L) or right (R) region (or several regions) which corresponds to the closes lying MAPER region of the MPA in the MNI template space.

Alzheimer's disease

The locations of the highest intensity on the atrophy map for the AD group includes the following MAPER regions: supramarginal and angular gyrus L (Figure 5.1), middle frontal gyrus R (Figure 5.2), posterior temporal lobe R and cerebellum R (Figure 5.3), superior parietal gyrus and cuneus R (Figure 5.4), anterior temporal lobe medial part L (Figure 5.5) and lateral remainder occipital lobe R.

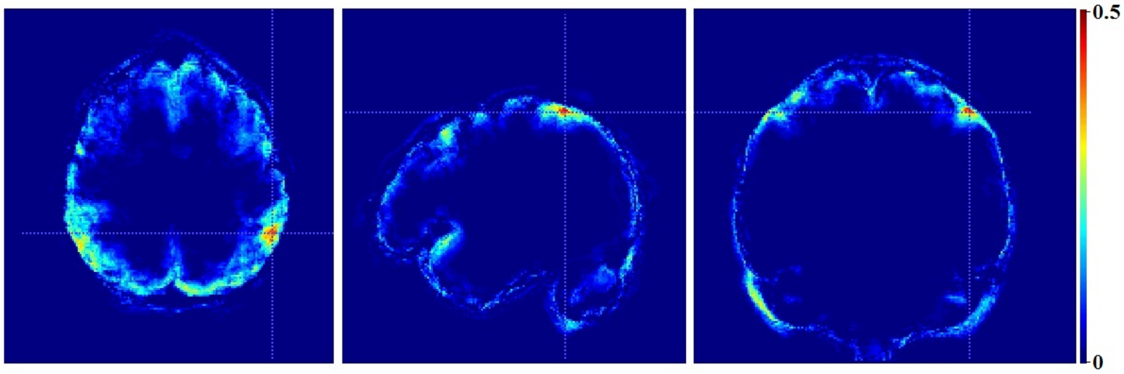

Figure 5.1: AD: supramarginal and angular gyrus L.

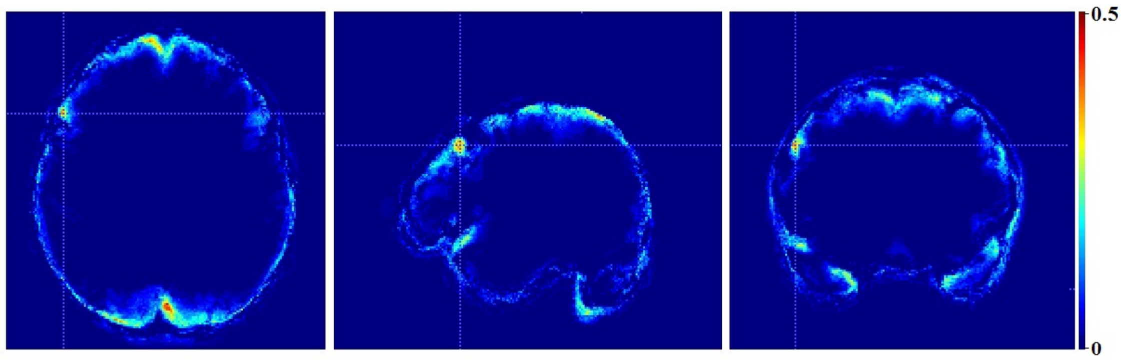

Figure 5.2: AD: middle frontal gyrus R.

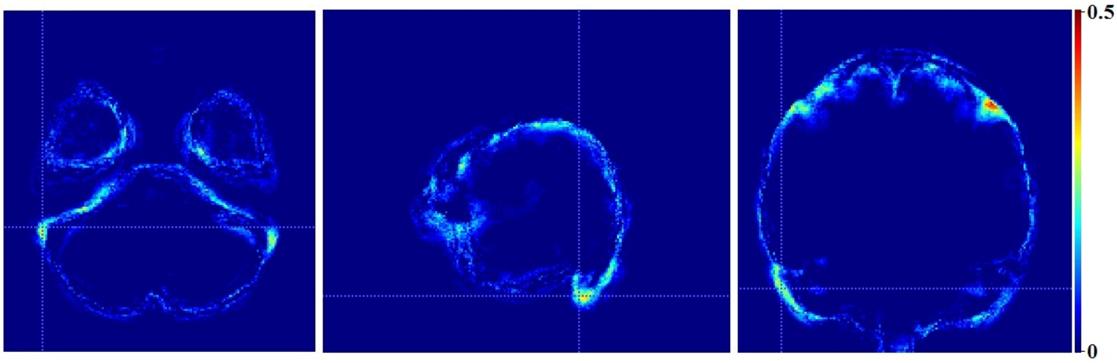

Figure 5.3: AD: posterior temporal lobe R and cerebellum R.

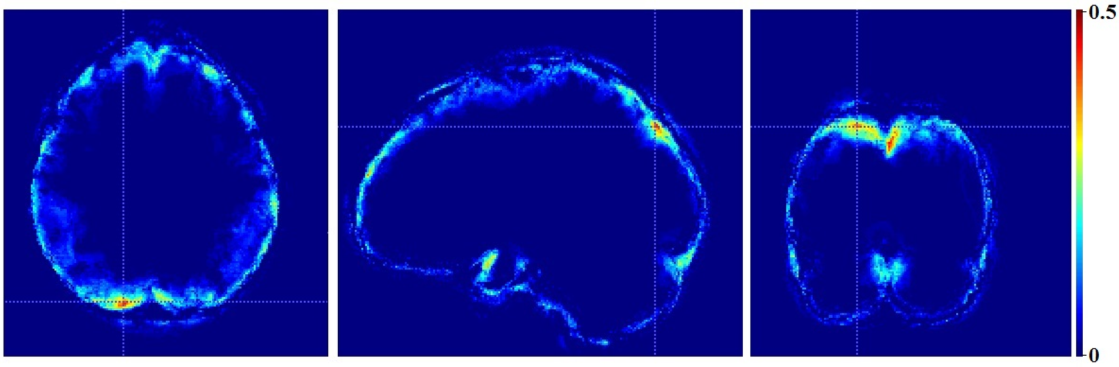

Figure 5.4: AD: superior parietal gyrus and cuneus R.

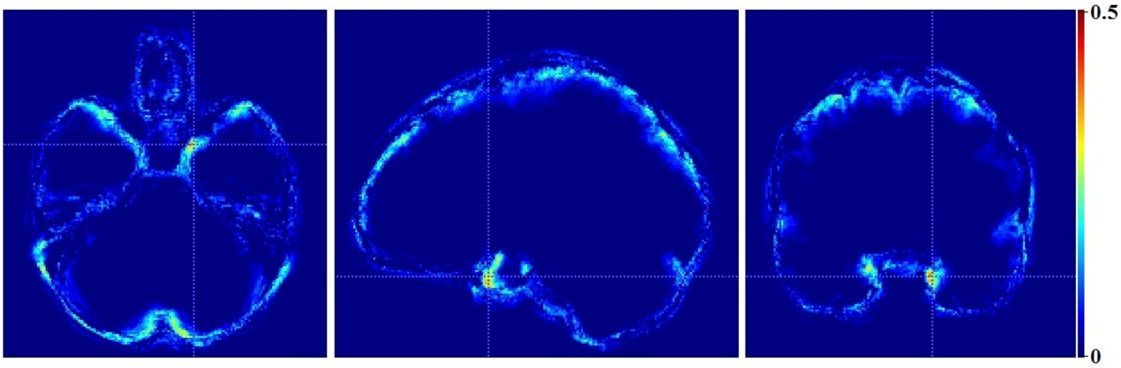

Figure 5.5: AD: anterior temporal lobe medial part L.

Mixed type of dementia (AD and VaD)

The most atrophied regions in Mix detected by the visualization method include the following brain regions: supramarginal gyrus L and postcentral gyrus L (Figure 5.7), middle frontal gyrus L (Figure 5.8), inferior frontal gyrus L (Figure 5.9), cerebellum L and R, lingual gyrus R, anterior temporal lobe medial part L and R, lateral remainder occipital lobe L and R and superior parietal gyrus L and R (all in Figure 5.6).

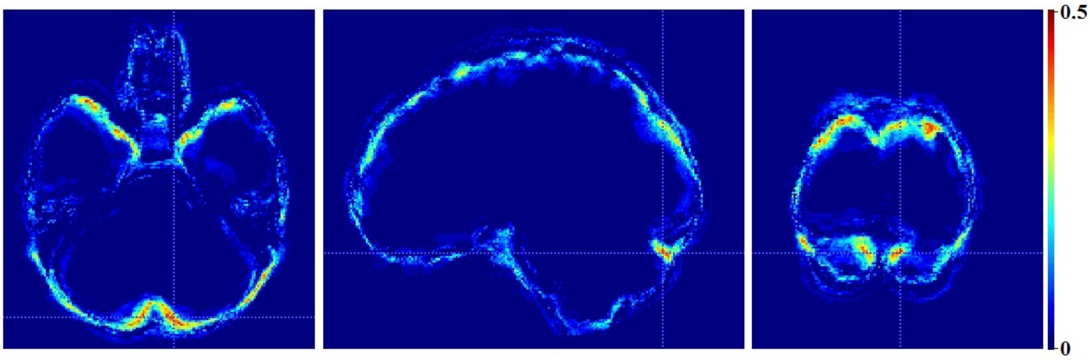

Figure 5.6: Mix: multiple regions.

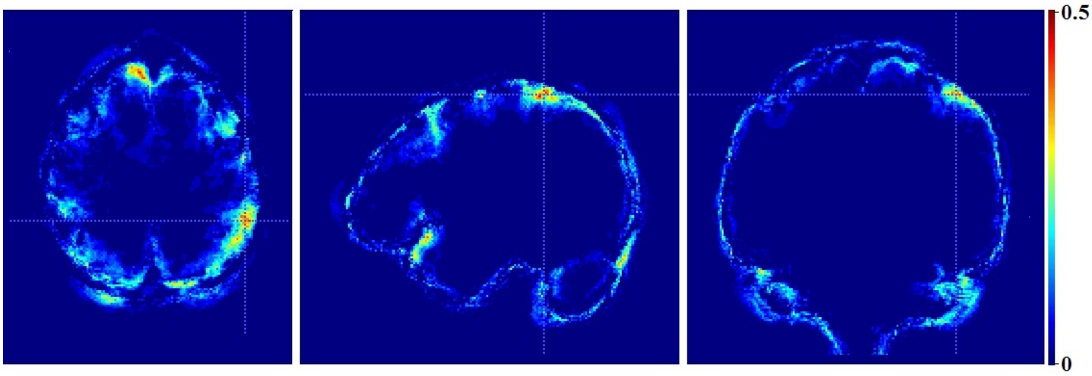

Figure 5.7: Mix: supramarginal gyrus L and postcentral gyrus L.

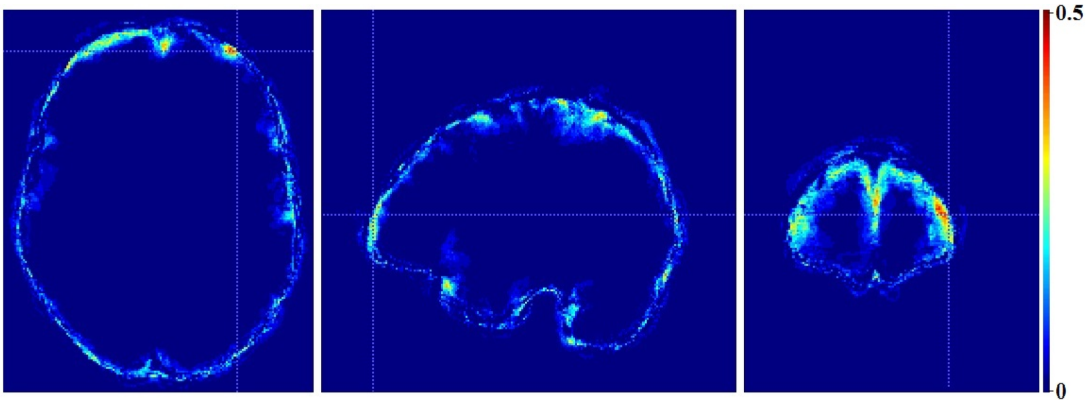

Figure 5.8: Mix: middle frontal gyrus L.

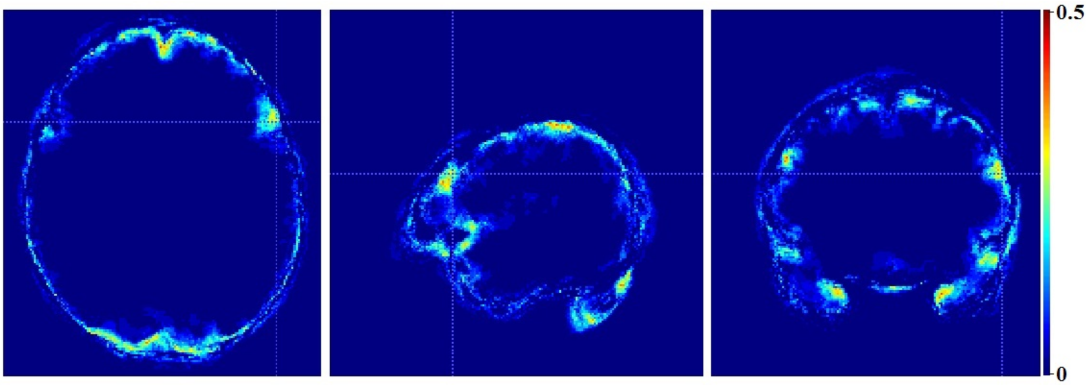

Figure 5.9: Mix: inferior frontal gyrus L.

Vascular dementia

The following regions were detected as the most atrophied with the visualization method: brainstem, cerebellum L and R, lingual gyrus L and R (Figure 5.10), precentral, postcentral and supramarginal gyri (all R, Figure 5.11), lateral remainder of occipital lobe R (Figure 5.12) and superior frontal gyrus L and R.

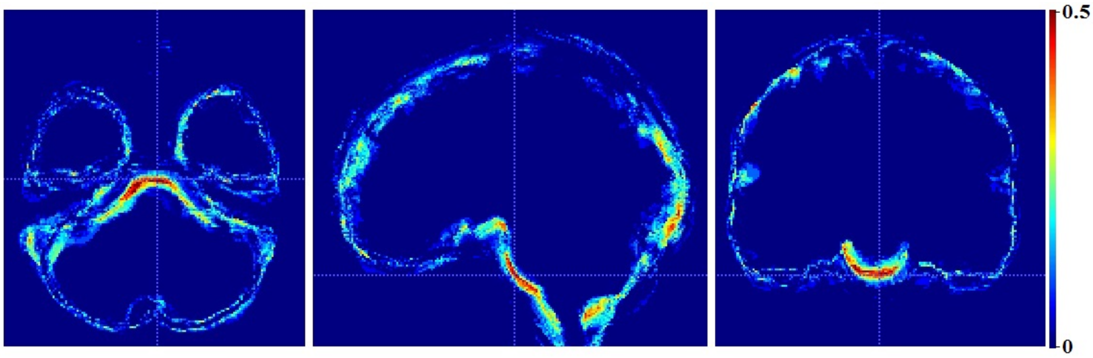

Figure 5.10: VaD: brainstem, cerebellum L and R, and lingual gyrus L and R.

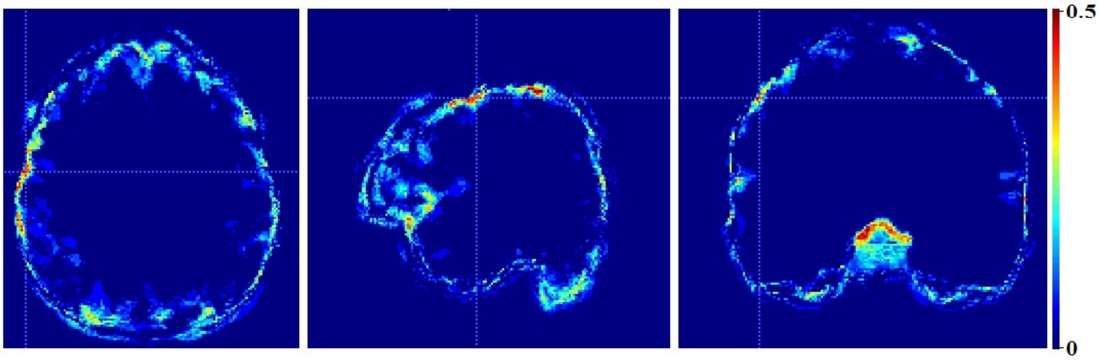

Figure 5.11: VaD: precentral, postcentral and supramarginal gyrus R.

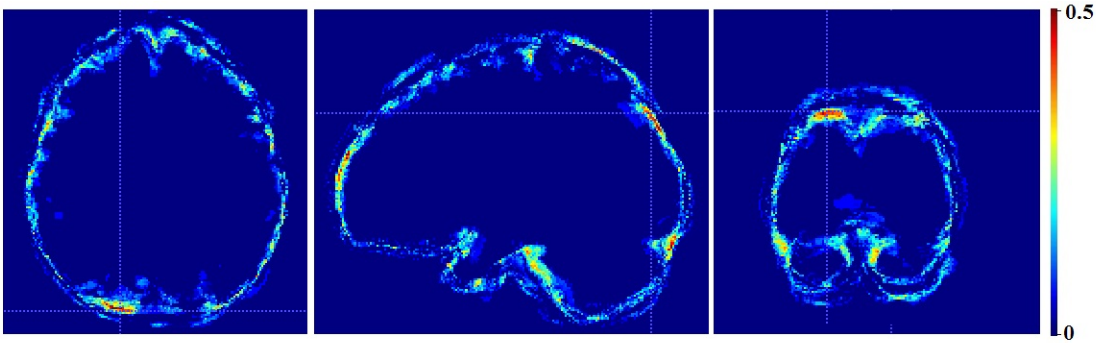

Figure 5.12: VaD: lateral remainder occipital lobe R.

Mix and VaD combined

The results for the combined vascular dementia and Mix groups obtained by the visualization method showed most atrophy in the following regions: parahippocampal and ambient gyrus R (Figure 5.13), superior parietal gyrus R (Figure 5.14), inferior frontal gyrus L (Figure 5.15), superior frontal gyrus R and lateral remainder occipital lobe L and R.

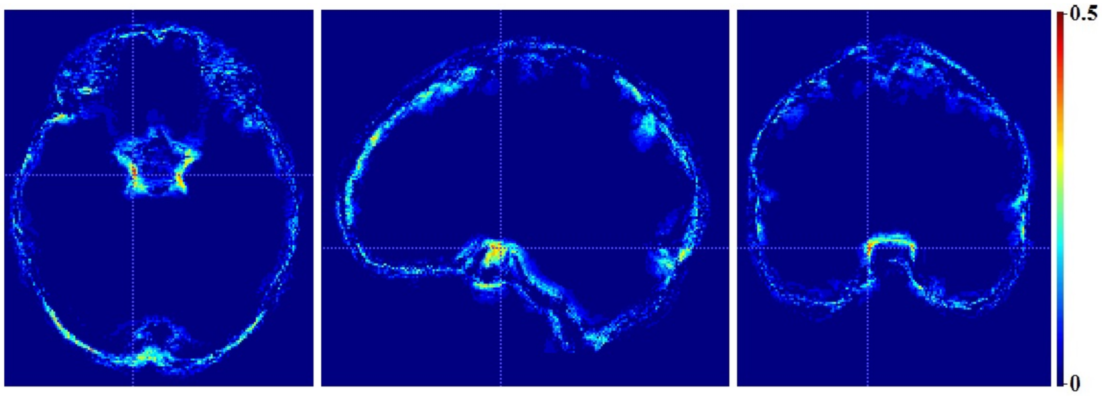

Figure 5.13: MVD: parahippocampal and ambient gyrus L and R.

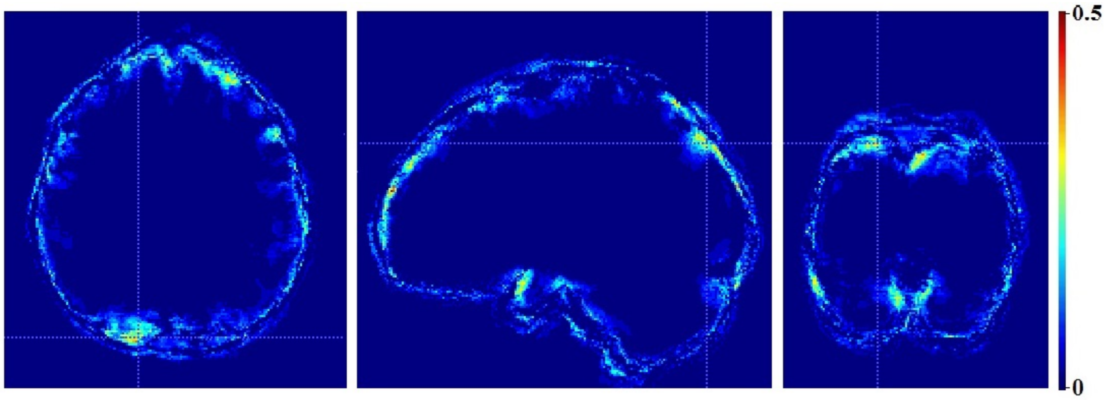

Figure 5.14: MVD: superior parietal gyrus R.

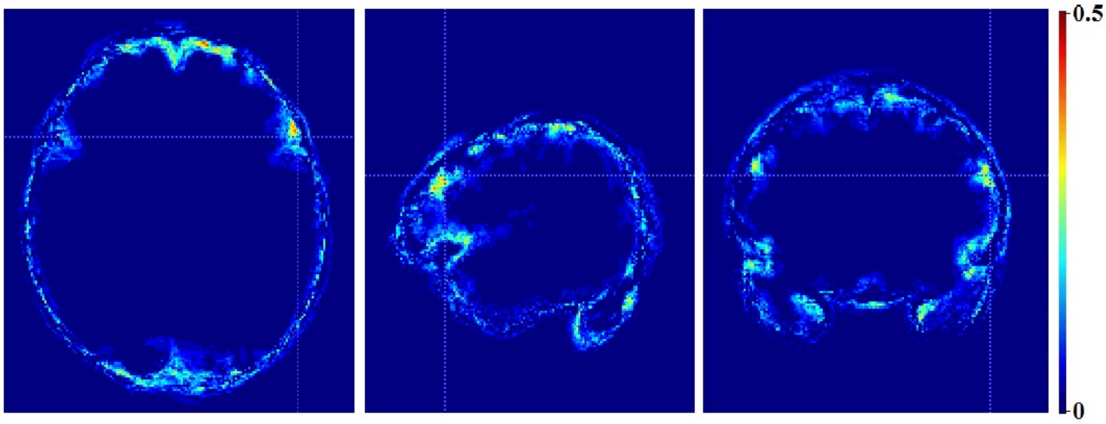

Figure 5.15: MVD: inferior frontal gyrus L.

Non-specified dementia

The following brain regions were found to be most atrophied with the visualization method: anterior temporal lobe medial part L (Figure 5.16), middle frontal gyrus R (Figure: 5.17) and superior parietal gyrus R (Figure 5.18).

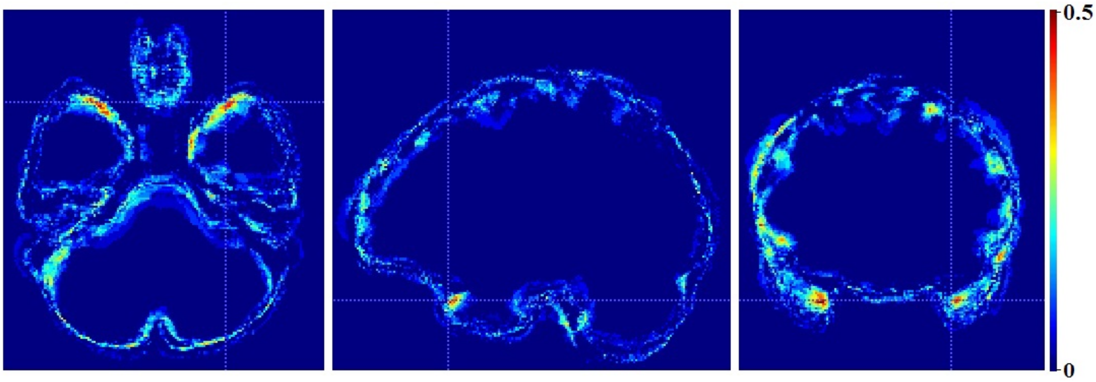

Figure 5.16: NUD: anterior temporal lobe medial part L.

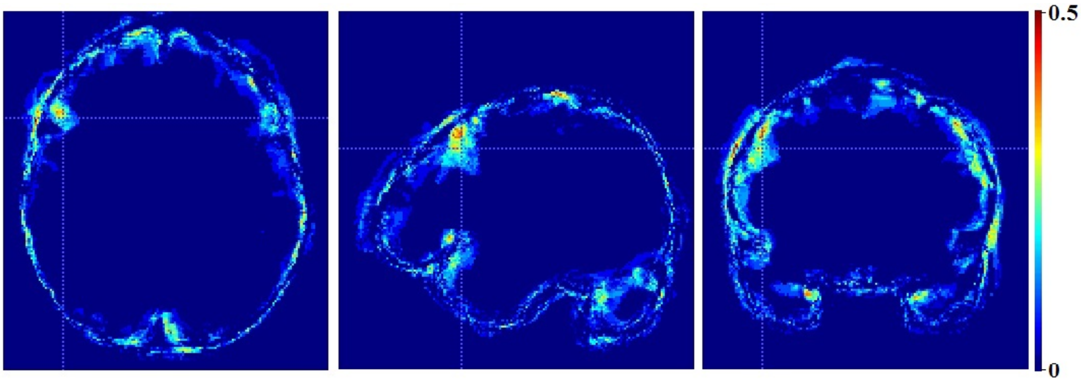

Figure 5.17: NUD: middle frontal gyrus R.

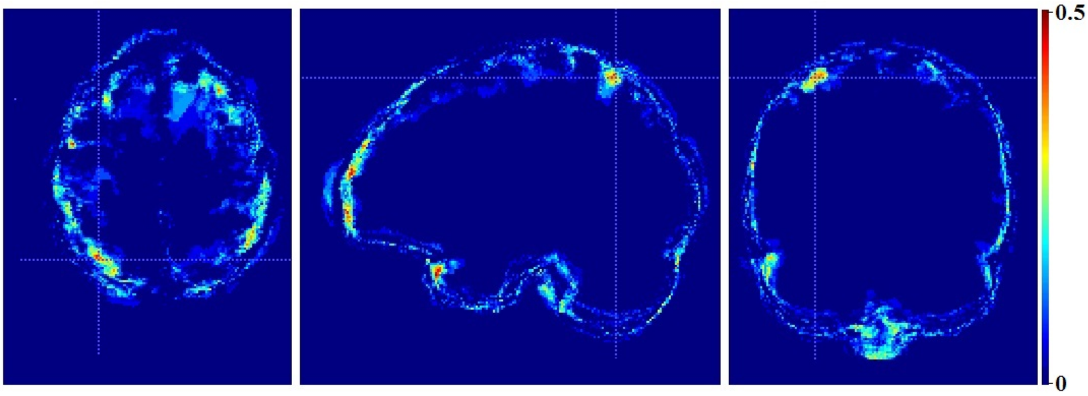

Figure 5.18: NUD: superior parietal gyrus R.

Mild and subjective cognitive impairment

A careful inspection of the visualization results obtained for MCI and SCI groups showed atrophy patterns which are similar in both these groups as well as in AD. The indicated locations include lateral remainder occipital lobe R, (Figure 5.19) middle frontal gyrus R (Figure 5.20) and supramarginal gyrus L (Figure 5.21). The figures include visualization of those regions in AD, MCI and SCI groups.

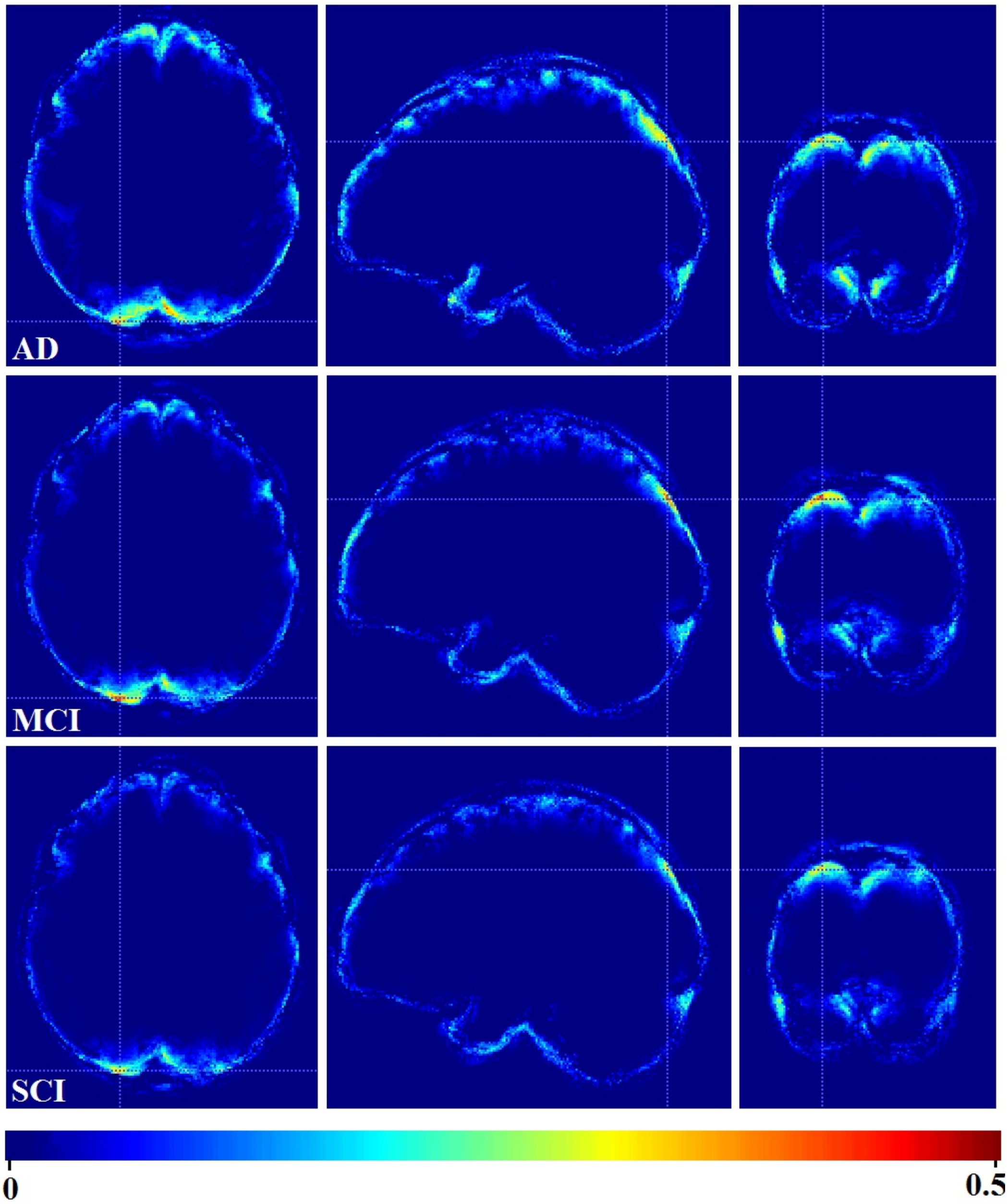

Figure 5.19: Lateral remainder occipital lobe R

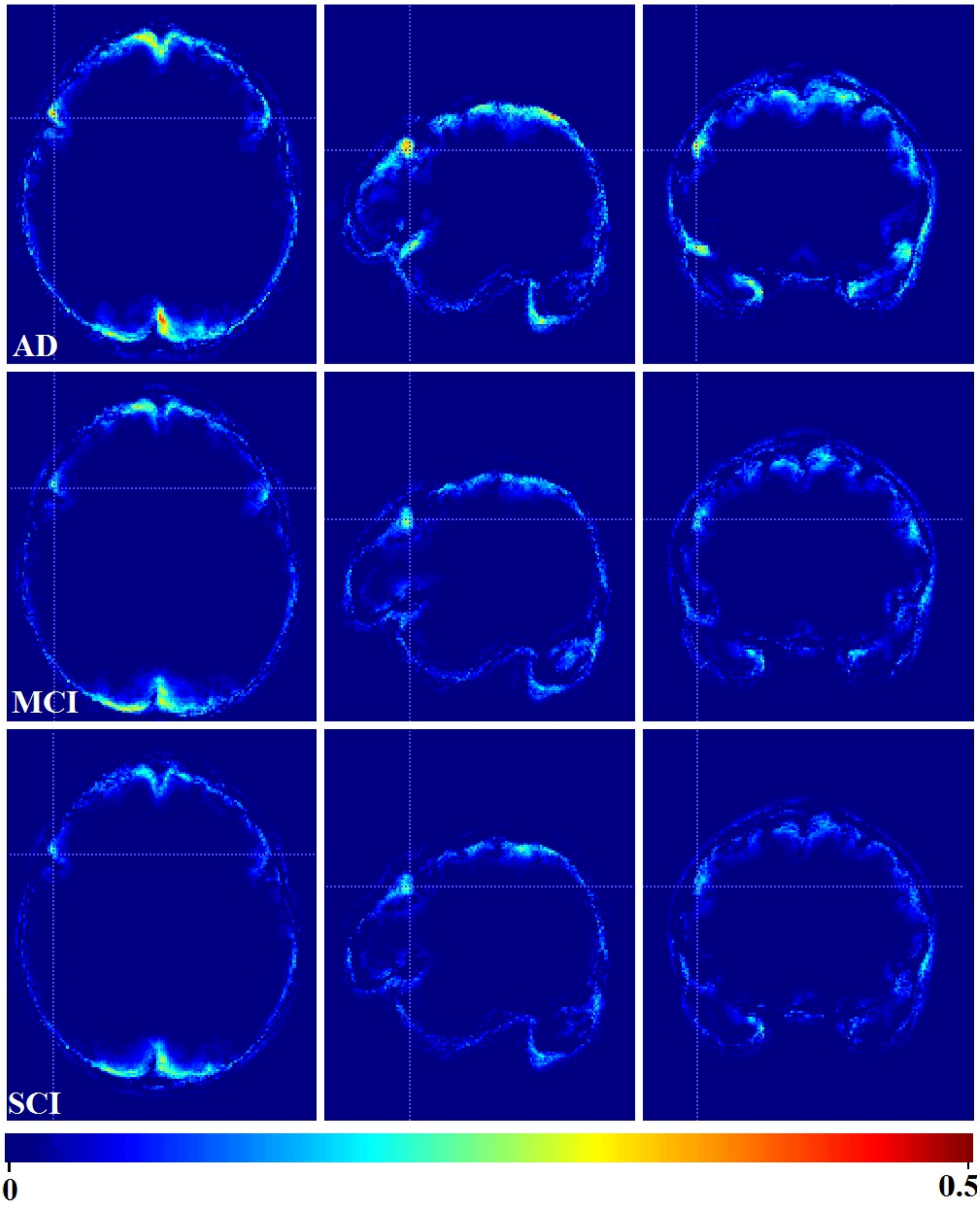

Figure 5.20: Middle frontal gyrus R

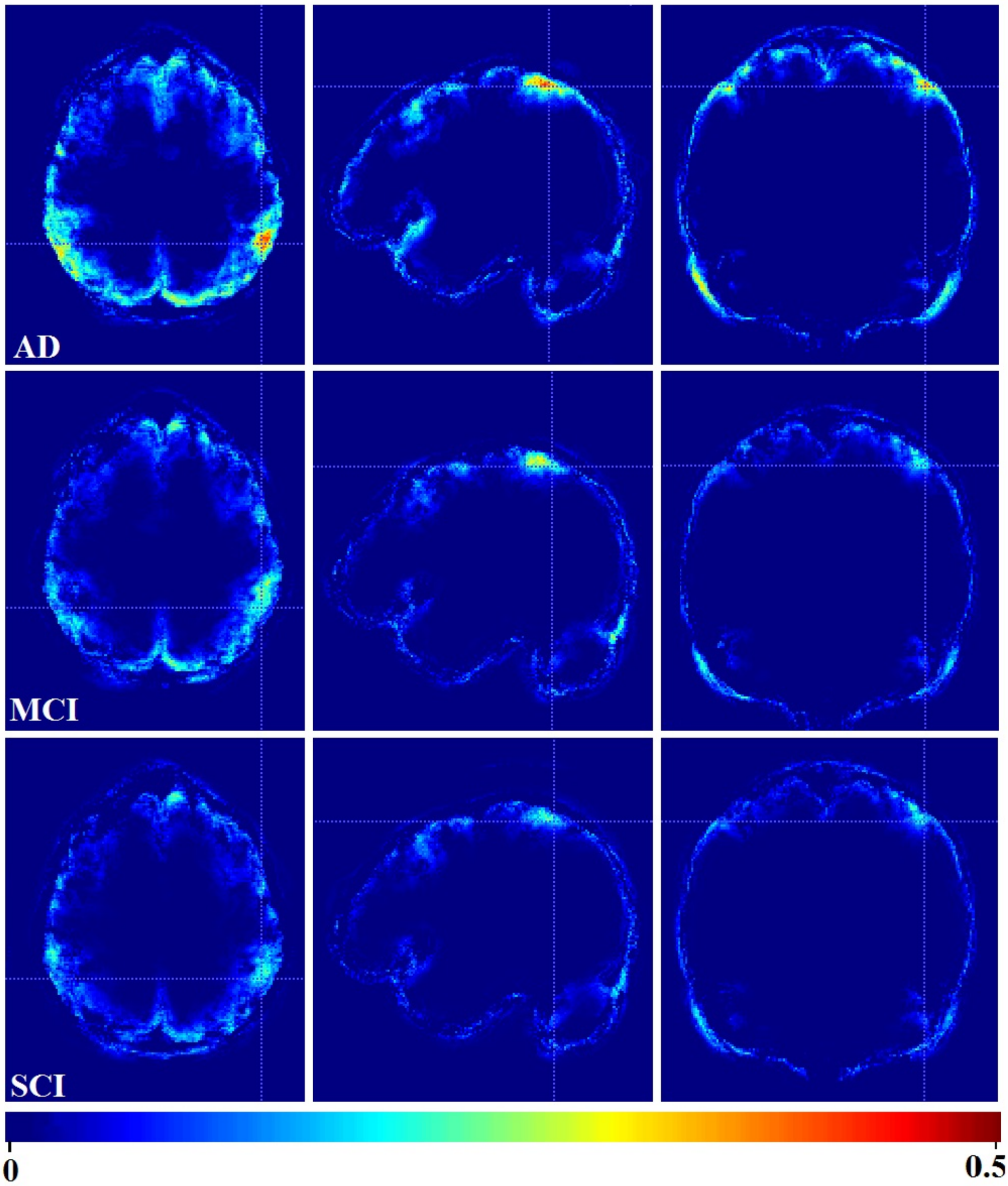

Figure 5.21: Supramarginal gyrus L

6

Discussion

The novel brain atrophy quantification method explored in this project detected significant atrophy at the regional level in three dementia groups: Alzheimer's disease, mixed-type of dementia, and vascular dementia combined with Mix. The last group was not originally included in the classification of the demented patients. The purpose of combining VaD and Mix was to increase the size of the sample of patients with vascular nature of neural degeneration. Both VaD and Mix groups contained patients who presented characteristics of vascular dementia white matter changes or coexisting frontal lobe signs and symptoms.

Whole-brain atrophy (Table 5.1) was largest in the Mix group (0.86) followed by AD (0.83) and MVD (0.80). The results for the remaining dementia groups were found not to be statistically significant, despite the atrophy scores suggesting increased DR volumes. The highest score in Mix is expected since two neurodegenerative processes are present, with both contributing to cortical atrophy. Furthermore, the mean age of the patients with Mix is higher than in AD (71.3 years versus 67.6 in AD). The atrophy score of the MVD group, which contains all patients with atrophy of vascular nature as well as the VaD group, is expected to be lower than for AD, however, only combining Mix and VaD resulted in significant atrophy. It is difficult to estimate which effect has the biggest contribution to the result: AD pathology in mixed-type dementia or increased sample size and mean age of the patients with vascular disease. A closer look at regional cortical atrophy in these groups shows similar areas of the cortex involved. The superior temporal gyrus middle part and the inferior frontal gyrus were found to be significantly atrophied in all three groups. Both AD and Mix showed significant atrophy in the cuneus and the posterior orbital gyrus. Both AD and MVD showed involvement of the angular gyrus (no parietal region was detected in Mix) and third ventricle. All atrophy scores of MVD regions were higher than the corresponding AD regions, contrary to what was found in the whole brain atrophy analysis. The Mix and MVD groups both showed significant atrophy in the middle and inferior temporal gyrus and the lateral remainder occipital lobe. The results coincide with the known location of atrophy occurring in AD. The presence of atrophy in parietal and occipital lobes may indicate a progressed case.

Another DR subregion that showed relative enlargement in dementia was the third ventricle. Although changes to this brain structure are observed in demented patients, this result may be considered implausible since the third ventricle is not located on the surface of the brain. The presence of this region points to some inaccuracies of the segmentation procedure and the input segmentations used. The

MAPER segmentation does not contain all known anatomical brain regions and the segmentation is less inclusive than the pincram brain mask. As a result there are superficial voxels that are labelled as brain by pincram, but that do not have any MAPER label. The neighbourhood of the third ventricle is the most prominent example since its bounding brain region is not labelled by MAPER, in which case the third ventricle becomes the closest label to the DR voxels lying in the neighbourhood. Atrophy of the regions unlabeled by MAPER will also contribute to an increase in third ventricle size, which aligns with the results.

Regions that were not significantly different from the control group also provide a valuable insight into the method. An outlier atrophy score was obtained for insula anterior short gyrus R (50.36) and subcallosal area R (13.18), and a relatively high score was observed for the left counterpart of subcallosal area (3.98) in patients with AD. Hypotheses testing supports the suspicion that such high scores are not a result of a far progressed atrophy of those regions but of a small sample size and outliers which increase the variance of examined distributions. A close inspection of the raw data reveals that insula anterior short gyrus L label was found in the DR of only two subjects with AD and 3 controls. The voxel count for the label was equal to one except for one AD patient (13), which explains the resultant atrophy score. A similar situation is observed for the subcallosal area. The right part was labelled in eight AD patients (mean voxel count equal to 11.75 and median equal to 2.5) and in 7 control patients (mean voxel count of 1.86 and median equal to 2). The left part of subcallosal area was found in 27 AD patients and 9 controls. The sample size can be considered sufficient in this case but the voxel count for that region is small enough that outliers will greatly increase the variance.

The VaD, NUD, and MCI groups had whole brain atrophy scores equal to 0.68, 0.65 and 0.43 and p-values equal to 0.1. Although not significant, it can be speculated that the brain undergoes more atrophy in MCI, NUD or VaD than in controls. The amount of atrophy detected with the method is not, however, sufficient to draw a significant conclusion. The SCI and ND groups did not show any significant difference to the control group (p-value=1). As noted for AD, the highest atrophy scores found for these groups correspond to regions which are labelled in only few subjects from each dementia group. The most frequently occurring of these regions is the subcallosal area.

Roughly half of the p-values calculated for regions in VaD group were equal to 1. The other half comprised mostly the temporal and frontal regions which also had the highest atrophy scores (Table 5.4). Although the results were not significantly different from the control group, involvement of those regions can be suspected. This speculation is supported by the diagnostic criteria for vascular dementia, which include frontal lobe symptoms, as well as atrophy patterns reported in the literature which resemble those of AD. A similar trend can be observed in NUD, where the regions with the highest atrophy scores and p-value < 0.5 are located in the frontal or the temporal lobe (Table 5.6). In the MCI group (Table 5.7), only two regions could be regarded as potentially involved in early stage of dementia: middle and inferior temporal gyrus L and cuneus R. In case of the SCI and ND groups (Tables 5.8 and 5.9), p-values for all regions were equal to 1, however the location of regions with the highest atrophy scores in SCI coincided with those found for MCI.

The FTD, LBD, PPA and Mix FTD/VaD groups did not have enough subjects to provide meaningful results, which is reflected in the values obtained from the volumetric analysis (extremely high atrophy score for FTD and conversely for Mix FTD/VaD, p-values equal to 1). Due to the insufficient sample size, hypothesis testing was not conducted for FTD, PPA, LBD and Mix FTD/VaD. Analyzing the atrophy scores of individual patients or a very small sample of patients can provide a perspective on the potential ability of this approach to detect a specific dementia type in a given patient. A closer look at the FTD group (Table 5.10) reveals that out of 19 regions with the highest atrophy scores (greater than 1), ten are located in the frontal lobe, eight are temporal lobe regions and the remaining one is insula anterior inferior cortex L. The majority of regions with the atrophy score greater than 1.5 (10 out of 13) are the frontal lobe regions. Those results coincide closely with the regions reported as mostly affected in this type of dementia. The examination of a scan of the patient with PPA (Table 5.10) shows involvement of four temporal regions, two frontal and one occipital in the group of most atrophied regions as detected by the method (atrophy score > 1.5). All of them are also found in the left hemisphere, which is expected in PPA. In LBD (Table 5.11), the highest atrophy scores (> 1.5) were found for temporal, parietal and frontal brain regions. The most atrophied one was superior temporal gyrus middle part L, which was also the most affected in AD. The patient diagnosed with Mix FTD/VaD (Table 5.11) showed a distinct atrophy (atrophy score > 1) in eight frontal regions and four temporal regions. The diagnosis criteria for VaD also include frontal lobe symptoms and, although not significant, the examination of the VaD group revealed high atrophy scores (greater than 1) for temporal regions as well. The results suggest that differentiation between the mixed type of dementia involving FTD and VaD and those individual conditions based on the cortical atrophy is a big challenge, since they seem to share common atrophy patterns. Although the results are not sufficient to make a conclusive diagnostic decision, they indicate that certain trends could be found in those groups and analyzing new sets with a sufficient number of patients diagnosed with these conditions could provide valuable insight into the cortical changes present in these dementia types.

The results of testing selected dementia pairs did not indicate any promising regions for distinguishing between different dementia types. Measuring cortical atrophy with the developed method may not be sensitive enough to find such regions, when the whole brain atrophy of two tested dementia groups is not substantially different. Another factor affecting the results could be the composition of the study cohort. A reliable test to find any patterns differentiating between AD and VaD, LBD or FTD requires sufficiently large sample sizes of each tested group. Comparing AD and VaD is of a particular interest and it requires a bigger VaD group. Combining VaD with Mix increased the sample size, but the influence of AD pathology in the mixed dementia group could reduce the ability of the method to detect atrophy due to vascular conditions.

Visualization results

The regions with the highest intensities coincide with the most significantly atrophied regions as detected in the numerical analysis . The most prominent changes were often spread between or closest to two or more MPA regions. Identification of the particular region contributing to the atrophy was thus difficult. One of the most atrophied regions found by the statistical analysis in AD, Mix, and MVD groups was inferior frontal gyrus R. This particular region was not identified in the visualization approach in any of these groups, but a neighbouring one, middle frontal gyrus R, revealed a high atrophy level in AD and Mix. With the affine registration, it is difficult to determine if it is only the middle frontal gyrus atrophy that contributes to the visual result. The example is shown in Figure 6.1. Similarly, the superior parietal gyrus R (Figure 5.4) is adjacent to the cuneus R and the supramarginal gyrus is neighbouring to the postcentral gyrus in AD and in Mix the area of high intensity located in the lingual gyrus lies next to cuneus. Lateral remainder occipital lobe was detected in both numerical analysis and visualization in Mix and MVD, although the intensity was smaller in the latter.

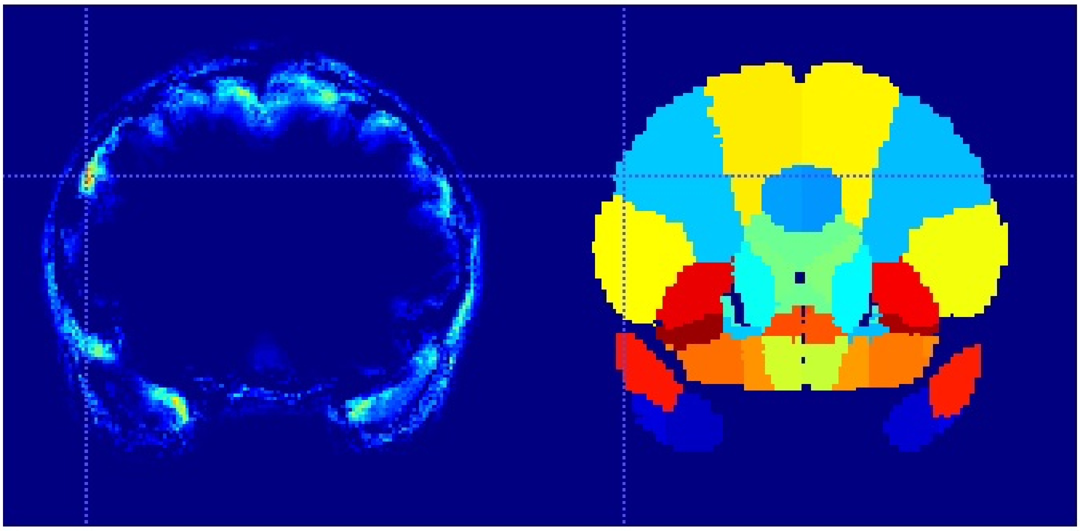

Figure 6.1: AD: the MPA regions in the neighbourhood of a highest intensity spot, middle frontal gyrus indicated by cross-hair and neighbouring inferior frontal gyrus (yellow) - coronal view.

The visualization of VaD showed regions of distinct atrophy not seen in the volume analysis. The most pronounced atrophy was found in brainstem. The region had a high atrophy score as well, however, the result was not significant. Due to a smaller number of patients included in this group, the visualization exhibits a very distinct but undesired effect of double edges (Figure 5.12). The effect is observed in all dementia groups, however the variation in registration are more visible in this case. The double edge could be also a result of making the warped DR masks of demented subjects consistently bigger than those of controls due to bigger brain atrophy. The registration applies a transformation matrix obtained from warping the intracranial volume to the MNI brain (Figure 3.3). The algorithm may be scaling up the atrophied brain to match the MNI brain and consequently scaling up the DR, with the scaling proportional to the head size but also the extent of atrophy. This could also be a reason for such discrepancies between volumetric analysis and visualization.

The visual examination of the images obtained for MCI and SCI (Figures 5.19 - 5.21) reveals patterns of atrophy which seem to be consistent in AD, MCI and SCI with a decreasing intensity (which corresponds to the level of atrophy) respectively. This could indicate the possibility of convergence of these particular study subjects. Especially in SCI and MCI, despite the absence of significantly atrophied regions, the highest atrophy scores were found for middle and inferior temporal gyrus L and R and precentral gyrus L in both groups. To support the supposition of convergence to AD, a longitudinal examination of these patients should be conducted, but this was outside the scope of this project. Visualization shows atrophy in regions that correspond to some of the known atrophy patterns in dementia. The approach, however, suffers from some inaccuracies, resulting from the affine registration. A coarse registration preserves the atrophied brain structure after normalization to a common space, but some variation in shape of particular brain regions remains. As a result the localization of the most important atrophy is only approximate.

The principle explored in this project estimates the extent of a given brain structure before the onset of atrophy. The approach can give an insight into the rate of degeneration, which can be particularly useful when longitudinal examinations are not available. The results presented show that the method is capable of detecting significant cortical atrophy in some regions whose involvement was reported in previous studies, but only in dementia groups that exhibit a pronounced whole brain atrophy in comparison to the control group, and only in groups that were sufficiently large. There were three such groups in the examined cohort. One of them contained patients diagnosed with AD alone and the remaining comprised patients with a certain degree of AD pathology involved as well. The results showed, that the influence of AD in the atrophy patterns is dominant in all these groups, and a distinction between them cannot be made based on the obtained results.

The method may benefit from modifications to increase its sensitivity. One is extending the MAPER segmentation with the missing anatomical structures or introducing an auxiliary label, which will complement the current MAPER segmentation so that it occupies the whole brain volume. The DR region in the neighbourhood will carry the auxiliary label, but the distribution of the remaining proper labels may change and influence the resultant values. Determining if the method is capable of distinguishing between pathology underlying different dementia types requires testing on larger, well characterized groups. The results obtained for individuals with FTD, LBD or PPA are encouraging – more tests with the method are warranted. At the same time, the cortical atrophy may not always be the most evident change in some dementia types and the method will not be suitable for making any definitive conclusions about characteristic atrophy patterns.

7

Conclusions

In this study, a new approach to quantify cortical brain atrophy at a regional level was developed and evaluated. The extent of atrophy is assessed by analyzing the discrepancy region that results from the subtraction of the brain region from the intracranial volume. This approach is based on a conjecture that the ICV represents an approximation of the maximum volume that the brain had before the onset of atrophy. The regional level of atrophy is calculated based on the discrepancy region segmentation, which labels DR voxels by proximity to the anatomical brain regions. The DR subregion volumes were normalized to ICV and standardized to the respective label volumes found in the control group or another dementia group. The volumes for each region were averaged across all subjects in a given study group. The resultant value was interpreted as the atrophy score for that brain region. A similar procedure was conducted on the DR volumes to calculate whole-brain atrophy for each dementia group. The results were tested against the hypothesis that the whole-brain and regional atrophy in dementia are different from those of the control group. A complementary visualization procedure was designed to show the locations of the most atrophied regions in different dementia types.

The results showed significant whole-brain atrophy in three dementia groups: mixed type of dementia (AD + VaD, atrophy score = 0.86), AD (atrophy score = 0.83), and vascular dementia combined with Mix (MVD, atrophy score = 0.80). Individual regions found to be significantly different from the control group in AD include (Table 5.2) superior temporal gyrus middle part (left), cuneus (right), angular gyrus (left), inferior frontal gyrus (right), posterior orbital gyrus (right) and postcentral gyrus (left). Significant involvement of the following regions was found in Mix (Table 5.3): middle and inferior temporal gyrus (left), inferior frontal gyrus (left), superior temporal gyrus middle part (left), cuneus (right), posterior orbital gyrus (right) and lateral remainder occipital lobe (right). The MVD (Table 5.5) showed significant deviation from the control group in inferior frontal gyrus (left), middle and inferior temporal gyrus (left), superior temporal gyrus middle part (left), middle and inferior temporal gyrus (right), angular gyrus (left), and lateral remainder occipital lobe. These patterns are similar, and considering the nature of degeneration in each of these groups, the AD involvement possibly dominates both in Mix and MVD groups.

Among the tested groups there were four which contained only one (or three) subjects: FTD (3 subjects), PPA, LBD and Mix FTD/VaD. The highest atrophy scores found in these subjects closely corresponded to the previously known patterns: frontal and temporal regions in FTD and Mix FTD/VaD, regions involved in

AD pathology in LBD, and regions from the left hemisphere in PPA.

The study offers a unique insight into the progression of cortical atrophy without a set of longitudinal scans, however the nature of the detected changes makes it more effective in cases of extensive atrophy, such as in AD. The conducted study reveals that the novel approach is not sensitive enough to distinguish regional differences in the examined dementia types. Nonetheless, its ability to detect expected regions in AD in comparison to the control group encourages further development of the method. Future work should focus on improving the segmentation approach, but more importantly the method should be tested on patient samples of sufficient size.

Bibliography

[1] Braak, Heiko, and Eva Braak. "Neuropathological stageing of Alzheimer-related changes." Acta neuropathologica 82.4 (1991): 239-259.

[2] Scahill, Rachael I., et al. "Mapping the evolution of regional atrophy in Alzheimer's disease: unbiased analysis of fluid-registered serial MRI." Proceedings of the National Academy of Sciences 99.7 (2002): 4703-4707.

[3] Yoshitake, T., et al. "Incidence and risk factors of vascular dementia and Alzheimer's disease in a defined elderly Japanese population The Hisayama Study." Neurology 45.6 (1995): 1161-1168.

[4] Wahlund, Lars-Olof, et al. "Imaging biomarkers of dementia: recommended visual rating scales with teaching cases." Insights into imaging (2016): 1-12.

[5] Barber, R., et al. "MRI volumetric study of dementia with Lewy bodies A comparison with AD and vascular dementia." Neurology 54.6 (2000): 1304-1309.

[6] Prince, M., et al. "World Alzheimer Report 2015. The global impact of dementia. An analysis of prevalence, incidence, cost & trends -Executive summary; Alzheimer's Disease International: London." (2015).

[7] Alzheimer's Association. "2017 Alzheimer's disease facts and figures." Alzheimer's & Dementia 13.4 (2017): 325-373.

[8] Schlesinger, Robert. "The Size of the U.S. and the World in 2016." Blog post. U.S. News., 05 Jan. 2016. Web. 08 May 2017. <https://www.usnews.com/opinion/blogs/robert-schlesinger/articles/2016-01-05/us-population-in-2016-according-to-census-estimates-322-762-018>.

[9] Colburn, W. A., et al. "Biomarkers and surrogate endpoints: Preferred definitions and conceptual framework. Biomarkers Definitions Working Group." Clinical Pharmacol & Therapeutics 69 (2001): 89-95.

[10] Varghese, Tinu, et al. "A review of neuroimaging biomarkers of Alzheimer's disease." Neurology Asia 18.3 (2013): 239.

[11] Chertkow, Howard, and Sandra Black. "Imaging biomarkers and their role in dementia clinical trials." The Canadian Journal of Neurological Sciences 34.S1 (2007): S77-S83.

[12] Erkinjuntti, Timo, et al. "Do white matter changes on MRI and CT differentiate vascular dementia from Alzheimer's disease?." Journal of Neurology, Neurosurgery & Psychiatry 50.1 (1987): 37-42.

[13] Bentley, Jon Louis. "Multidimensional binary search trees used for associative searching." Communications of the ACM 18.9 (1975): 509-517.

[14] Maneewongvatana, Songrit, and David M. Mount. "On the efficiency of nearest neighbor searching with data clustered in lower dimensions." International Conference on Computational Science. Springer Berlin Heidelberg, 2001.

[15] Redmond, Stephen J., and Conor Heneghan. "A method for initialising the K-means clustering algorithm using kd-trees." Pattern recognition letters 28.8 (2007): 965-973.

[16] Saha, Sriparna, and Sanghamitra Bandyopadhyay. "MRI brain image segmentation by fuzzy symmetry based genetic clustering technique." Evolutionary Computation, 2007. CEC 2007. IEEE Congress on. IEEE, 2007.

[17] Ilunga-Mbuyamba, Elisee, et al. "Localized active contour model with background intensity compensation applied on automatic MR brain tumor segmentation." Neurocomputing 220 (2017): 84-97.

[18] Almeida, Diogo F., et al. "Fully automatic segmentation of femurs with medullary canal definition in high and in low resolution CT scans." Medical Engineering & Physics 38.12 (2016): 1474-1480.

[19] Heckemann, Rolf A., et al. "Brain extraction using label propagation and group agreement: pincram." PloS one 10.7 (2015): e0129211.

[20] Schnabel, Julia A., et al. "A generic framework for non-rigid registration based on non-uniform multi-level free-form deformations." International Conference on Medical Image Computing and Computer-Assisted Intervention. Springer, Berlin, Heidelberg, 2001.

[21] Rueckert, Daniel, et al. "Nonrigid registration using free-form deformations: application to breast MR images." IEEE transactions on medical imaging 18.8 (1999): 712-721.

[22] Denton, Erika RE, et al. "Comparison and evaluation of rigid, affine, and nonrigid registration of breast MR images." Journal of computer assisted tomography 23.5 (1999): 800-805.

[23] Heckemann, Rolf A., et al. "Improving intersubject image registration using tissue-class information benefits robustness and accuracy of multi-atlas based anatomical segmentation." Neuroimage 51.1 (2010): 221-227.

[24] Barber, R., et al. "Volumetric MRI study of the caudate nucleus in patients with dementia with Lewy bodies, Alzheimer's disease, and vascular dementia." Journal of Neurology, Neurosurgery & Psychiatry 72.3 (2002): 406-407.

[25] Patro, Satya Narayana, et al. "Role of neuroimaging in multidisciplinary approach towards Non-Alzheimer's dementia." Insights into imaging 6.5 (2015): 531-544.

[26] Ahmed, R. M., et al. "Biomarkers in dementia: clinical utility and new directions." Journal of Neurology, Neurosurgery & Psychiatry (2014): jnnp-2014.

[27] Biagioni, Milton C., and James E. Galvin. "Using biomarkers to improve detection of Alzheimer's disease." (2011).

[28] Knopman, David S., et al. "Evolution of neurodegeneration-imaging biomarkers from clinically normal to dementia in the Alzheimer disease spectrum." Neurobiology of Aging 46 (2016): 32-42.

[29] Menéndez González, Manuel. "Atlas of Biomarkers for Alzheimer's Disease", Springer International Publishing, 2014, DOI: 10.1007/978-3-319-07989-9. Accessed 01.06.2017.

[30] Takahashi, R., et al. "Measurement of gray and white matter atrophy in dementia with Lewy bodies using diffeomorphic anatomic registration through exponentiated lie algebra: a comparison with conventional voxel-based morphometry." American Journal of Neuroradiology 31.10 (2010): 1873-1878.

[31] Whitwell, Jennifer L., et al. "Focal atrophy in dementia with Lewy bodies on MRI: a distinct pattern from Alzheimer's disease." Brain 130.3 (2007): 708-719.

[32] Dementia | Signs, Symptoms & Diagnosis
http://www.alz.org/what-is-dementia.asp

[33] Schneider, Lon S., Vicki E. Pollock, and Scott A. Lyness. "A metaanalysis of controlled trials of neuroleptic treatment in dementia." Journal of the American Geriatrics Society 38.5 (1990): 553-563.

[34] Boxer, Adam L., and Bradley F. Boeve. "Frontotemporal dementia treatment: current symptomatic therapies and implications of recent genetic, biochemical, and neuroimaging studies." Alzheimer Disease & Associated Disorders 21.4 (2007): S79-S87.

[35] Burton, E. J., et al. "Patterns of cerebral atrophy in dementia with Lewy bodies using voxel-based morphometry." Neuroimage 17.2 (2002): 618-630.

[36] Nedelska, Zuzana, et al. "Pattern of brain atrophy rates in autopsy-confirmed dementia with Lewy bodies." Neurobiology of aging 36.1 (2015): 452-461.

[37] Brenneis, Christian, et al. "Basal forebrain atrophy is a distinctive pattern in dementia with Lewy bodies." Neuroreport 15.11 (2004): 1711-1714.

[38] Cousins, D. A., et al. "Atrophy of the putamen in dementia with Lewy bodies but not Alzheimer's disease An MRI study." Neurology 61.9 (2003): 1191-1195.

[39] Hanyu, Haruo, et al. "Differences in MR features of the substantia innominata between dementia with Lewy bodies and Alzheimer's disease." Journal of neurology 252.4 (2005): 482-484.

[40] Frisoni, Giovanni Battista, et al. "Brain atrophy in frontotemporal dementia." Journal of Neurology, Neurosurgery Psychiatry 61.2 (1996): 157-165.

[41] Kipps, Christopher M., et al. "Clinical significance of lobar atrophy in frontotemporal dementia: application of an MRI visual rating scale." Dementia and geriatric cognitive disorders 23.5 (2007): 334-342.

[42] Sung, Young-Hee, et al. "Midbrain atrophy in subcortical ischemic vascular dementia." Journal of neurology 256.12 (2009): 1997.

[43] Van de Pol, Laura, et al. "Hippocampal atrophy in subcortical vascular dementia." Neurodegenerative Diseases 8.6 (2011): 465-469.

[44] Apostolova, Liana G., et al. "Conversion of mild cognitive impairment to Alzheimer disease predicted by hippocampal atrophy maps." Archives of neurology 63.5 (2006): 693-699.

[45] Grundman, Michael, et al. "Brain MRI hippocampal volume and prediction of clinical status in a mild cognitive impairment trial." Journal of Molecular Neuroscience 19.1 (2002): 23-27.

[46] Misra, Chandan, Yong Fan, and Christos Davatzikos. "Baseline and longitudinal patterns of brain atrophy in MCI patients, and their use in prediction of short-term conversion to AD: results from ADNI." Neuroimage 44.4 (2009): 1415-1422.

[47] Henneman, W. J. P., et al. "Hippocampal atrophy rates in Alzheimer disease Added value over whole brain volume measures." Neurology 72.11 (2009): 999-1007.

[48] Devanand, D. P., et al. "Hippocampal and entorhinal atrophy in mild cognitive impairment prediction of Alzheimer disease." Neurology 68.11 (2007): 828-836.

[49] Hammers, Alexander, et al. "Three-dimensional maximum probability atlas of the human brain, with particular reference to the temporal lobe." Human brain mapping 19.4 (2003): 224-247.

[50] Gousias, Ioannis S., et al. "Automatic segmentation of brain MRIs of 2-year-olds into 83 regions of interest." Neuroimage 40.2 (2008): 672-684.

[51] Faillenot, Isabelle, et al. "Macroanatomy and 3D probabilistic atlas of the human insula." NeuroImage 150 (2017): 88-98.

[52] Chang, Che-Wei, Chien-Chang Ho, and Jyh-Horng Chen. "ADHD classification by a texture analysis of anatomical brain MRI data." Frontiers in systems neuroscience 6 (2012): 66.

[53] Rueckert, Daniel, et al. "Nonrigid registration using free-form deformations: application to breast MR images." IEEE transactions on medical imaging 18.8 (1999): 712-721.

[54] Jenkinson, Mark, et al. "Fsl." Neuroimage 62.2 (2012): 782-790.

[55] Grabner, Günther, et al. "Symmetric atlasing and model based segmentation: an application to the hippocampus in older adults." Medical Image Computing and Computer-Assisted Intervention–MICCAI 2006 (2006): 58-66.

[56] Jenkinson, Mark, and Stephen Smith. "A global optimisation method for robust affine registration of brain images." Medical image analysis 5.2 (2001): 143-156.

[57] Jenkinson, Mark, et al. "Improved optimization for the robust and accurate linear registration and motion correction of brain images." Neuroimage 17.2 (2002): 825-841.

[58] Andersson, Jesper LR, Mark Jenkinson, and Stephen Smith. "Non-linear registration, aka Spatial normalisation FMRIB technical report TR07JA2." FMRIB Analysis Group of the University of Oxford 2 (2007).

[59] Wallin, Anders, et al. "The Gothenburg MCI study: design and distribution of Alzheimer's disease and subcortical vascular disease diagnoses from baseline to 6-year follow-up." Journal of Cerebral Blood Flow & Metabolism 36.1 (2016): 114-131.

[60] Auer, Stefanie, and Barry Reisberg. "The GDS/FAST staging system." International Psychogeriatrics 9.S1 (1997): 167-171.

[61] Klasson, Niklas, et al. "Valid and efficient manual estimates of intracranial volume from magnetic resonance images." BMC medical imaging 15.1 (2015): 5.

[62] Weber, Roger, Hans-Jörg Schek, and Stephen Blott. "A quantitative analysis and performance study for similarity-search methods in high-dimensional spaces." VLDB. Vol. 98. 1998.

[63] Moore, Andrew W. "An intoductory tutorial on kd-trees." (1991).

[64] Benjamini, Yoav, and Daniel Yekutieli. "The control of the false discovery rate in multiple testing under dependency." Annals of statistics (2001): 1165-1188.

[65] Holm, Sture. "A simple sequentially rejective multiple test procedure." Scandinavian journal of statistics (1979): 65-70.

A

Appendix

Normalized Mutual Information

Normalized mutual information is a voxel-based similarity measure, which allows estimating the degree of alignment of two images. Mutual information (MI) between two images is expressed as an amount of information contained in one image (A) about the second image (B) and given by equation A.1 [53]

$$MI(A,B) = H(A) + H(B) - H(A,B), \tag{A.1}$$

where $H(A)$ and $H(B)$ is entropy of images A and B respectively, and $H(A,B)$ is joint entropy of A and B. The entropy of a discrete random variable X (intensity of image A) is defined a:

$$H(X) = -\sum_{x} p(x) log_2 p(x), \tag{A.2}$$

where $p(x)$ is the probability mass function of X, $P(X = x)$. The joint entropy of A and B is defined as:

$$H(X) = -\sum_{x}\sum_{y} p(x,y) log_2 p(x,y), \tag{A.3}$$

where $p(x,y)$ is joint probability mass function of X and Y, $P(X = x \text{ and } Y = y)$, and Y is the intensity of image B.

The normalized mutual information is then defined as [53]:

$$NMI(A,B) = \frac{H(A) + H(B) - H(A,B)}{H(A,B)}. \tag{A.4}$$

Rigid image registration

Rigid image registration has 6 DoF, which allow three translations along x, y and z axes of the image space and three rotations by α, β and γ about those axes respectively. Each voxel (v_x, v_y, v_z) of the atlas image is mapped to the target space using the following relation:

$$\begin{pmatrix} v'_x \\ v'_y \\ v'_z \\ 1 \end{pmatrix} = R \begin{pmatrix} v_x \\ v_y \\ v_z \\ 1 \end{pmatrix} + t$$

where R is a product of matrices R_α, R_β and R_γ which rotate a given point by α, β and γ and t is the translation vector by along axes x, y and z:

$$R_\alpha = \begin{pmatrix} 1 & 0 & 0 & 0 \\ 0 & cos(\alpha) & sin(\alpha) & 0 \\ 0 & -sin(\alpha) & cos(\alpha) & 0 \\ 0 & 0 & 0 & 1 \end{pmatrix}, R_\beta = \begin{pmatrix} cos(\beta) & 0 & sin(\beta) & 0 \\ 0 & 1 & 0 & 0 \\ -sin(\beta) & 0 & cos(\beta) & 0 \\ 0 & 0 & 0 & 1 \end{pmatrix}, R_\gamma = \begin{pmatrix} cos(\gamma) & sin(\gamma) & 0 & 0 \\ -sin(\gamma) & cos(\gamma) & 0 & 0 \\ 0 & 0 & 1 & 0 \\ 0 & 0 & 0 & 1 \end{pmatrix}$$

and

$$t = \begin{pmatrix} t_x \\ t_y \\ t_z \\ 1 \end{pmatrix}$$

Affine image registration

Affine transformation adds stretching in an arbitrary direction to the transformations performed by the rigid registration. The affine mapping of a point (v_x, v_y, v_z) to a target space is represented by the following relation:

$$\begin{pmatrix} v'_x \\ v'_y \\ v'_z \\ 1 \end{pmatrix} = \begin{pmatrix} a_x & b_x & c_x & t_x \\ a_y & b_y & c_y & t_y \\ a_z & b_z & c_z & t_z \\ 0 & 0 & 0 & 1 \end{pmatrix} \begin{pmatrix} v_x \\ v_y \\ v_z \\ 1 \end{pmatrix},$$

where $a, b, andc$ are variables containing information about rotation, scaling and shearing around respective axes.